A scenario-based integrated battery sizing and power plant scheduling under variable fuel prices and maritime operational profiles

Durgaprasad, Sankarshan; Coraddu, Andrea; Heyneman, Eben; Lamproye, Christof; Polinder, Henk

DOI
10.1016/j.ecmx.2025.101240

Publication date
2025

Document Version
Final published version

Published in
Energy Conversion and Management: X

Energy Conversion and Management: X 28 (2025) 101240

Contents lists available at ScienceDirect

Energy Conversion and Management: X

journal homepage: www.sciencedirect.com/journal/energy-conversion-and-management-x

A scenario-based integrated battery sizing and power plant scheduling under variable fuel prices and maritime operational profiles

Sankarshan Durgaprasad [a,*], Andrea Coraddu [a], Eben Heyneman [b], Christof Lamproye [b], Henk Polinder [a]

[a] Faculty of Mechanical Engineering, Delft University of Technology, Mekelweg 2, 2628 CD Delft, South Holland, The Netherlands
[b] Jan De Nul nv, Tragel 60, Hofstade-Aalst, 9308, Belgium

ARTICLE INFO

Keywords:
Energy management
Hybrid power system
Lithium ion battery
Mixed integer linear programming
Optimization
Power plant scheduling
Stochastic

ABSTRACT

Hybrid power systems are increasingly adopted onboard. Lithium-ion batteries now serve as a viable energy storage solution that enhances fuel efficiency and reduces the operating hours of main power units, thereby reducing operational expenses. However, integrating batteries onboard requires decision-making that accounts for diverse scenarios, including battery chemistry, variations in vessel operational profiles, and fluctuating fuel prices. To address these challenges, this study investigates whether battery sizing and scheduling of the power and energy management system require a scenario-based stochastic decision framework. Specifically, it examines how energy storage requirements are influenced by varying load profiles, whether the optimal battery size and power management strategy are affected by fuel price fluctuations, and how robust the overall strategy remains under operational uncertainties. A deterministic equivalent of a two-stage stochastic decision framework is introduced to incorporate these uncertainties, offering insights into the required battery technology, capacity, and correlated behavior of onboard energy management. Multiple scenarios are applied to a trailing suction hopper dredger, analyzing three load profiles with distinct variations in power demand. With reserve power constraints enforced, the optimal battery capacity remains fixed. However, when these constraints are relaxed, the optimal battery size becomes more sensitive to fuel price changes. In addition, the results showcase reduction in diesel engine operating hours—thereby lowering both fuel consumption and maintenance costs, demonstrating that these operational benefits depend not only on the battery's size but also on its available throughput, which allows for deeper cycling.

1. Introduction

Batteries on board vessels serve various functions and offer multiple benefits, with most achieving payback periods of less than five years for many vessel types, making them an attractive environmental and economic investment [1]. Depending on the type of vessel and its operational profile, batteries can be utilized in different ways. For example, they can reduce diesel engine (DE) usage, thereby lowering operating hours and greenhouse gas emissions [2]. They can also act as a spinning reserve for dynamic positioning vessels or enable optimal loading of primary power sources on board [3], among other applications. Traditionally, the maritime industry has relied on mode-based or rule-based control systems [4]. However, recent studies on optimal vessel control aim to minimize operational expenses based on fuel consumption, emissions and battery degradation [5–8]. This suggests that optimal control or system scheduling can have a varied impact depending on fluctuations in operational costs. Over recent years, fuel costs in the maritime industry have varied significantly, as shown in Fig. 1. The figure illustrates the distribution of fuel prices at the Port of Rotterdam [9]. These fuel price fluctuations represent just one of the many uncertainties affecting maritime operations, which also include diverse operational needs and environmental influences.

The maritime industry comprises a diverse range of vessels, each with unique operational needs [10]. Within each vessel segment, ships may perform various tasks, operate under different profiles [11] influenced by factors such as weather conditions [12,13], or function in multiple modes of operation [14]. This variability introduces significant uncertainty in decision-making, particularly when determining the appropriate energy and power sources on board or identifying the most effective operational strategy. Uncertainty thus arises from varying fuel prices, technology costs and investment decisions, as well as diverse operational requirements [15,16].

* Corresponding author.
E-mail address: s.durgaprasad@tudelft.nl (S. Durgaprasad).

https://doi.org/10.1016/j.ecmx.2025.101240
Received 11 June 2025; Received in revised form 24 August 2025; Accepted 30 August 2025
Available online 7 September 2025

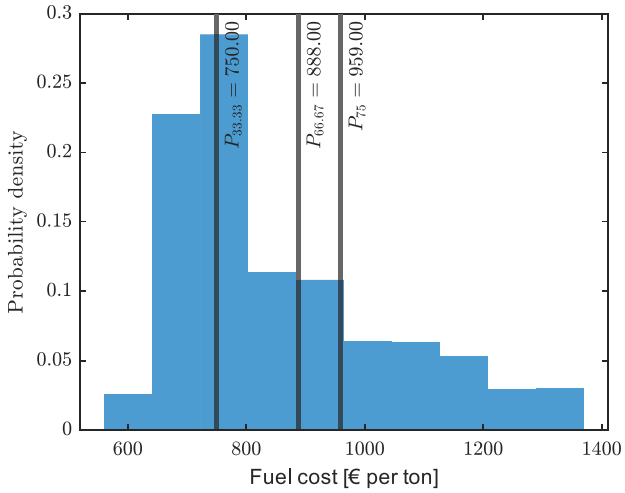

Fig. 1. Rotterdam bunker fuel price from 07/03/2022-05/03/2025 [9]. Where P_x refers to the xth percentile of the fuel price distribution.

This study focuses on hybridizing an existing power plant of a trailing suction hopper dredger (TSHD) under the uncertainty of operational profiles and expenses. Three distinct load profiles are used, each under two different fuel price scenarios, resulting in a consideration of six scenarios. Furthermore, six cases are formulated, comprising a wide range of probable operational situations. Lithium-ion batteries are selected for hybridization due to their superior overall performance, including higher energy and power densities, longer cycle life, and cost effectiveness compared with alternative energy storage solutions for maritime applications [17,18]. Among lithium-ion batteries, lithium nickel manganese cobalt oxide (NMC) and lithium–titanium–oxide (LTO) batteries are preferred for high power applications [10]. Consequently, these battery types are considered in this study.

Based on the literature review in Section 2, two critical research gaps are identified in the context of hybrid maritime power plants operating under uncertainty.

GAP 1 The joint influence of fuel price volatility and operational variability on the design requirements of maritime energy storage systems has not been systematically investigated.

GAP 2 Existing studies overlook how such uncertainties affect the optimal scheduling of power and energy systems, particularly when battery degradation through lifetime throughput constraint is considered.

To address these gaps, this study explores whether the sizing and scheduling of hybrid maritime power and energy systems necessitate a scenario-based stochastic decision-making framework. Specifically, it investigates how energy storage requirements vary under diverse load conditions, quantifies the sensitivity of optimal battery sizing to fuel price fluctuations, and analyzes the impact of such economic uncertainties on the power and energy management strategy. Furthermore, the robustness of the resulting strategy is evaluated against operational variability, with particular attention to mission-dependent load profiles and battery throughput characteristics.

This paper presents a decision-oriented framework for analyzing the influence of operational variability – such as fuel costs, load profiles, and battery technologies – on the sizing of energy storage systems and the scheduling of hybrid maritime power systems. Rather than focusing on selecting a single optimal battery size or chemistry, the study emphasizes how these factors interact to shape system requirements and control strategies.

The contributions of this work are fourfold. First, it introduces a deterministic equivalent of a two-stage stochastic optimization framework tailored for joint battery sizing and energy–power plant scheduling in the presence of fuel price and operational uncertainties specific to maritime applications. Second, it proposes a flexible and extendable optimization approach capable of handling multiple maritime load profiles and a range of fuel price scenarios, enabling adaptive scheduling strategies under uncertainty. Third, through the evaluation of six distinct cases across six scenarios, the study reveals that battery sizing requirements are shaped not only by operational profiles and fuel price levels, but also by battery chemistry, which plays a critical role in defining optimal scheduling behavior. Finally, it demonstrates how effective battery throughput management strategies can be implemented across diverse maritime missions and economic conditions, offering actionable insights for robust and adaptable power plant scheduling.

The rest of the paper is structured as follows. Section 2 discusses the existing literature on hybrid power plants, energy storage, and stochastic decision-making frameworks, providing the basis for this research. Section 3 presents the onboard power system and operational characteristics, detailing the benchmark and proposed system topologies. Section 4 describes the scenario generation process and outlines the methodology used for optimization, including formulating different operational and fuel price scenarios. Section 5 introduces the mathematical model, covering the objective function, power balance equations, DE and battery constraints. Section 6 presents the results and discussion, analyzing the performance of the proposed approach under various scenarios and evaluating the impact of operational uncertainties. Section 7 concludes the study by summarizing key findings, discussing implications, and suggesting future research directions.

2. Related work

The problem of optimally sizing energy storage systems for maritime applications is well established, whether the focus is on fully electric vessels or hybrid power plants [19–27]. While these studies offer valuable insights, the majority do not fully account for the uncertainties associated with operations and operational expenditure in the maritime applications, and only a small number of studies have tried to address these complexities.

When uncertainty has been studied, it has been approached in various ways within the literature. For instance, in [11], the authors synthesize four distinct operational profiles from measured load data to examine the optimal sizing of system components alongside their energy management strategies. Their study explores how different operational profiles and emission reduction targets influence hybridization design for a particular type of vessel. A two-layer optimization approach is adopted, with the outer layer minimizing capital expenditure (CAPEX) and the inner layer focusing on reducing operational expenses (OPEX) and formulating the control strategy. Although this method effectively captures the operational strategy for a given load profile, it may not fully account for the diverse range of missions a vessel could undertake in practice, nor for uncertainties such as fluctuating fuel costs.

A two-stage probabilistic risk-averse approach for energy storage system sizing in all-electric ships, which integrates both investment and operational considerations, is presented in [13]. The authors employ Kernel Density Estimation to model environmental uncertainties and jointly optimize multi-objective energy storage system sizing and energy management scheduling while incorporating hydrodynamic constraints. However, the study does not account for battery lifetime during operation. While stochasticity in the load profile is considered, battery degradation is omitted, meaning the model does not prioritize energy and power management across different scenarios based on degradation factors. Furthermore, the authors use a single base load profile, introducing stochasticity only within that predefined framework, rather than considering multiple diverse load profiles.

The framework developed in [14] considers multiple operational profiles, modes of operation, and battery energy throughput. It provides insights into operational differences due to variations in load profiles,

the combined effect of load profile variability and investment cost, and the impact of load fluctuations on battery throughput. The study offers a comprehensive understanding of energy storage requirements under these conditions. However, the authors do not examine the combined variability of operational profiles with other key factors, such as fuel prices or maintenance-related OPEX. These elements are crucial, as fuel price fluctuations and maintenance costs influence operational strategies.

The variability in operational profiles is addressed in [28], where the authors develop a representative load profile based on a year-long operational dataset, using the most frequently observed load ramps and power levels. Additionally, a predefined low-pass filter strategy is applied to determine the power split between onboard sources, enabling the calculation of degradation incurred by the fuel cell and battery. Using this approach, 14 different scenarios are analyzed to assess lifetime design and determine the net present value of the retrofitted fuel cell-battery propulsion system compared to the existing system. Such a study is beneficial to analyze the power split for a given load profile and a method to synthesis representative profiles, however, it fails to determine when to competitively use the battery system in a hybrid power system given the different scenarios.

The uncertainty in battery technology (cost, energy density), fuel and electricity prices, and volume opportunity cost for a battery-electric container ship is examined in [16]. The authors analyze 45 vessels across four propulsion technologies (ICE, NMC, LFP, LTO batteries) over passage lengths of 500–20,000 km, using a 3×3 scenario matrix that combines carbon pricing with technology development. Their approach provides a holistic perspective on the potential adoption of battery-electric container ships, both now and in the future. This study highlights the necessity of considering different scenarios and variability in such assessments.

In [29] the uncertainties in solar radiation and load demand are addressed by employing a two-stage stochastic optimization model for determining the optimal sizing of a hybrid photovoltaic/diesel/storage power system for merchant marine vessels. Solar radiation uncertainty is modeled through a Monte Carlo simulation to generate a wide range of scenarios, which are then reduced using a scenario reduction technique to manage computational complexity. The model incorporates five operational load modes for the vessel, reflecting different scenarios such as cruising or docking, to account for varying energy demands.

While only a limited number of maritime studies have addressed energy storage system requirements under uncertainty, whether through case-based scenario analysis or stochastic optimization frameworks [11,13,14,16,28,29], such approaches are well-established in the broader context of large-scale energy storage systems in terrestrial and grid-connected applications.

A stochastic model for optimal planning of battery energy storage systems for an isolated microgrid is presented in [30]. The uncertainties considered in their model include renewable energy generation (solar radiation and wind speed) and power demand. These uncertainties are modeled through probabilistic scenarios to capture variability, employing Monte Carlo simulations. Additionally, uncertainties related to battery operation, such as capacity degradation over time, are also included. The time step of consideration used for operational analysis in the paper is one hour.

A stochastic optimization model for renewable-based microgrid operation incorporating battery operating cost is presented in [31]. Uncertainties include renewable generation variability (solar and wind) and load forecasting errors, modeled via a probabilistic constrained approach. Battery-related uncertainties like efficiency losses, capacity degradation, and lifecycle costs are also incorporated. The operational analysis uses hourly intervals.

A risk-averse two-stage stochastic model for retailer planning, incorporating self-generation and storage systems, is presented in [32]. The uncertainties considered include electricity pool market prices and consumer demand, modeled using scenario-based analysis to handle variability and manage risk. The time step considered for operational analysis is one hour. A similar two-stage stochastic optimization framework for isolated hybrid microgrids in a rural system is presented in [33]. The uncertainties considered include variability in renewable energy resources, specifically solar generation, and stochastic variations in rural electricity consumption. These uncertainties are modeled using probabilistic methods, historical monitoring data, and synthetic stochastic scenarios generated. Additionally, uncertainties related to the performance and efficiency of system components such as batteries and diesel generators are included. The time step considered for operational analysis in the paper is hourly intervals.

Large-scale two-stage or multi-stage stochastic optimization frameworks often deploy decomposition techniques to exploit the block structure between first-stage and second-stage decisions [34,35]. However, since this work involves a relatively small number of scenarios, we can leverage this advantage by directly formulating the two-stage stochastic optimization problem in its deterministic equivalent form.

These examples from literature [30–33] illustrate the diversity of stochastic optimization frameworks previously applied to onshore energy systems. However, extending these frameworks to maritime systems is challenging due to fundamental differences in system dynamics. Maritime systems, although similar in power levels to onshore microgrids, feature dynamics that operate on much shorter timescales, from seconds to minutes, depending on battery functions and DE's capable of transitioning between ON and OFF states in a matter of minutes. Consequently, the half-hourly or hourly intervals commonly adopted in onshore stochastic optimization are inadequate for maritime applications, as these intervals cannot capture the rapid charging and discharging cycles of batteries nor the complex, short-term operational constraints and unit commitment decisions of onboard DEs.

3. Onboard power system and operation

The data acquired for this study come from an existing vessel with mechanical propulsion. However, newer versions of the same vessel are equipped with electrical propulsion, as shown in Fig. 2(a). The base power of the system is taken as 8000 kW. The electrically propelled version of this vessel shall be considered the benchmark. The system comprises three DE units, two with a capacity of 0.5 p.u. and an auxiliary DE with a capacity of 0.123 p.u. The goal is to address the research objectives posed in Section 1 by integrating a battery system, as shown in Fig. 2(b). The vessel also has multiple non-propulsive loads, as illustrated in Fig. 2, which are active during dredging and dumping operations.

Two different load profiles, where the TSHD is in operation, are considered, along with one load profile representing periods when the TSHD is out of operation. The dredging and dumping operations can be observed in the operational profiles shown in Figs. 3(a) and 3(b). The load profile on Fig. 3(a) involves extended propulsion periods between the dredging and dumping cycles. The dredging cycle is characterized by an increase in hopper load, whereas the dumping cycle is identified by a decrease in hopper load. A relatively constant hopper load indicates that the TSHD is sailing. The second load profile, shown in Fig. 3(b), has minimal time between the dredging and dumping cycles, resulting in a shorter overall cycle compared to the first load profile. The load profile when the vessel is out of operation is shown in Fig. 3(c). The power demand during such an operation is significantly lower as compared to when the vessel is operational. Moreover, only DE-3 (auxiliary DE) is operational during this period.

The distribution of power between the DE's for the operational load profiles is shown in Figs. 4(a) and 4(b). A contrast can be observed between the power distribution for load profile 1 (Fig. 4(a)) and load profile 2 (Fig. 4(b)). In load profile 1, DE-1 and DE-2 are relatively well loaded compared to load profile 2. For load profile 1, DE-1 operates above 60% for 59.9% of the time, while DE-2 is loaded above 60% for 53.3% of the time. In contrast, for load profile 2, these percentages drop

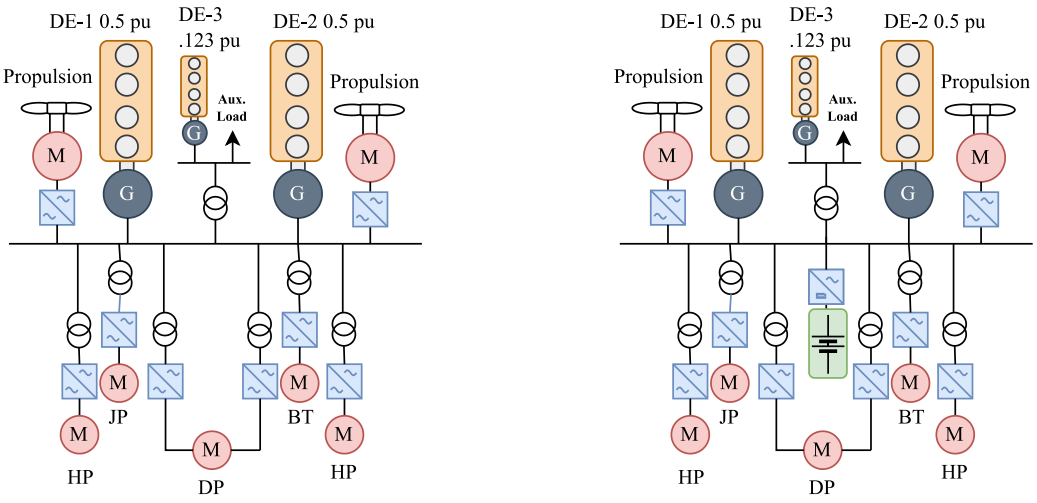

(a) Benchmark topology

(b) Proposed topology

Fig. 2. Comparison of benchmark and proposed topology.

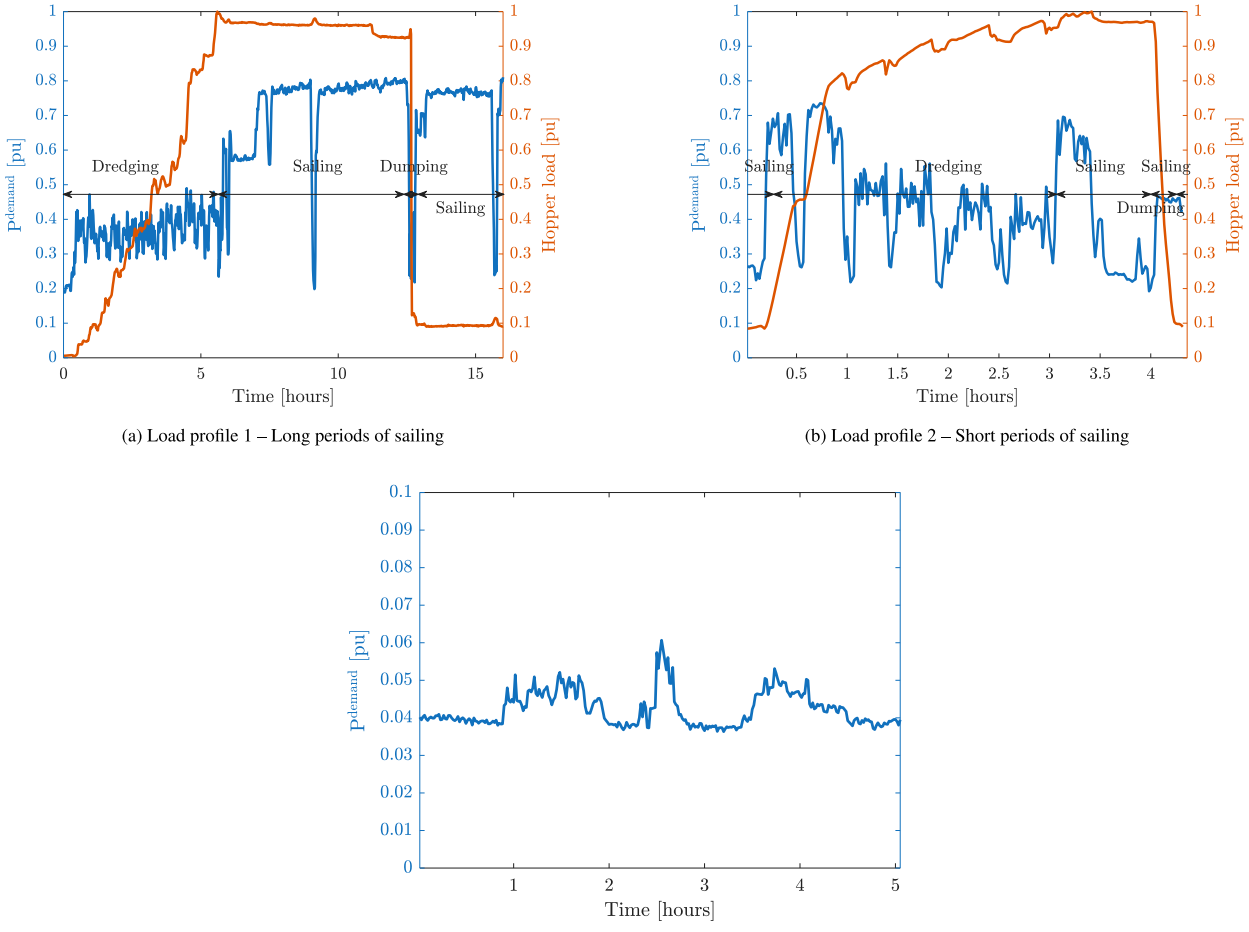

(a) Load profile 1 – Long periods of sailing

(b) Load profile 2 – Short periods of sailing

(c) Load profile 3 – Operation at port

Fig. 3. Three load-profile plots arranged in a triangular layout: (a) Long periods of sailing, (b) Short periods of sailing, and (c) Operation at port.

to 35.5% and 20.8% for DE-1 and DE-2, respectively. This highlights the significant difference between the two operational profiles and suggests a greater potential for improving fuel efficiency in the second load profile. Similarly, the histogram of the auxiliary (AUX) DE loading during periods when the vessel is out of operation is shown in Fig. 4(c), where the AUX DE operates under low loading conditions.

The fuel consumption of the DE's can be estimated using the specific fuel oil consumption (SFOC) curves typically provided by the manufacturer, as shown by the original SFOC data points (kg/kWh) in Fig. 5. Interpolating these data points results in a second-order relationship between DE load and fuel consumption, as illustrated by the quadratic fit curve. However, these curves can be adjusted by multiplying the data

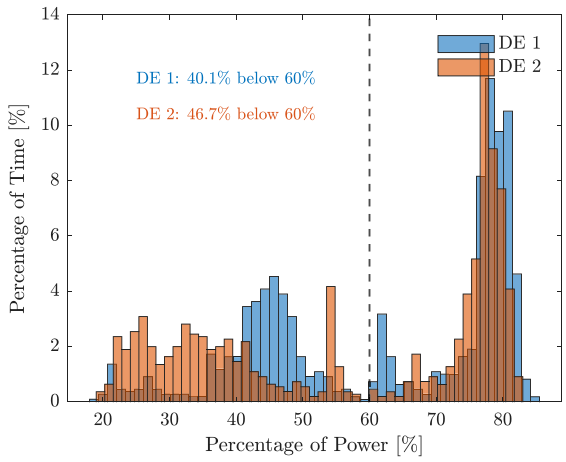

(a) Histogram of DE loading for load profile 1

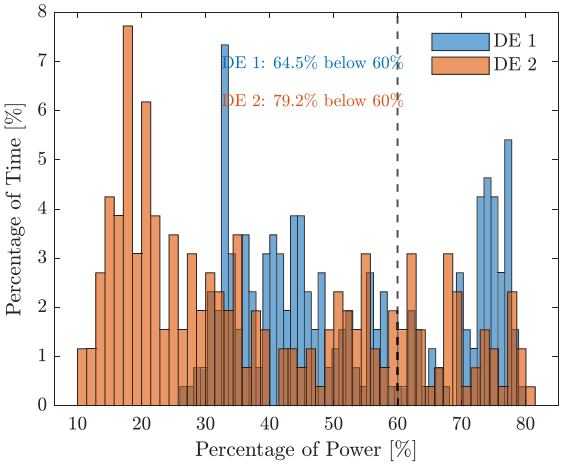

(b) Histogram of DE loading for load profile 2

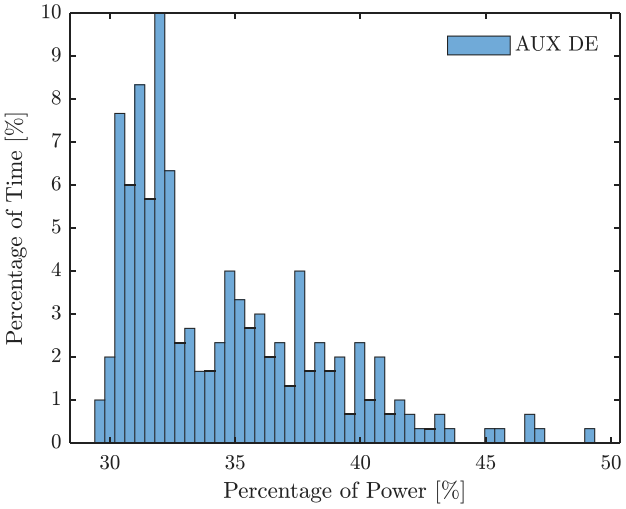

(c) Histogram of DE loading for load profile 3

Fig. 4. Histograms of DE loading arranged in a triangular layout: (a) Load profile 1, (b) Load profile 2, and (c) Load profile 3.

points by the corresponding power, yielding the fuel consumption flow (kg/h), as shown in Fig. 5. Furthermore, interpolating these adjusted data points results in a linear relationship between power demand and fuel consumption flow (kg/h) [14], represented by the linear fit line in Fig. 5. In addition to the fuel consumption, there are maintenance costs (C^{maint}) associated with the running hours of the DE. For this specific vessel, the associated costs are considered to be €30 per hour of operation for DE-1 and DE-2 and €7.5 per hour for the DE 3 (AUX DE).

4. Optimization framework and scenario design

This section presents the overall optimization methodology and the structure of the scenario and case generation process. Section 4.1 introduces the four-step modeling and solution framework used to determine battery sizing and onboard scheduling strategies under uncertainty. Section 4.2 then details the design of a structured scenario matrix and associated cases, used to explore the interaction between fuel price volatility, mission-dependent load profiles, and battery chemistries in a tractable yet representative manner.

4.1. Optimization methodology

The methodological workflow developed to address the research objectives is illustrated in Fig. 6. It consists of four key steps, designed to systematically integrate scenario generation, optimization, and techno-economic evaluation. In the first step, raw vessel load profile data are analyzed and preprocessed to remove inconsistencies and ensure temporal alignment. This provides a clean and representative set of operational conditions for downstream modeling. In the second step, discrete scenarios are constructed by combining variations in mission-dependent load profiles with fuel price fluctuations. These scenarios are grouped into multiple cases, each representing a distinct realization of operational and economic conditions. In the third step, the deterministic equivalent of a two-stage stochastic optimization problem is formulated and solved for each case. The first-stage decision

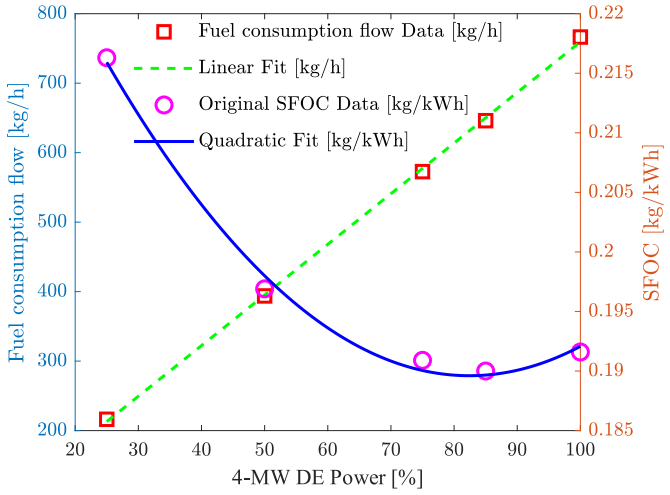

Fig. 5. Specific fuel consumption curve of 4-MW DE onboard. Coefficient values provided in Table 4.

corresponds to the sizing of the battery system, while the second-stage recourse actions govern the power and energy scheduling across the scenario tree. The onboard hybrid energy system is modeled using a Mixed-Integer Linear Programming (MILP) formulation. The optimization objective $\mathcal{O}$ minimizes the total lifetime cost – including capital expenditures, operational expenditures, and degradation-related costs – subject to system constraints and degradation limits. This process is performed for two representative battery chemistries: LTO and NMC. Finally, the fourth step involves a financial post-analysis, where key performance indicators such as Payback Period and Return on Investment (ROI) are computed for each case–chemistry pair. The complete implementation logic is summarized in Algorithm 1.

The optimization is carried out using the academic license of Gurobi, with solver version 12.0.1 [36].

Algorithm 1 : Implementation of methodology

```
for chem in {LTO, NMC} do                    ▷ Select battery chemistry
    for case in {1,...,12} do                ▷ Select case
        Solve the optimization problem to minimize 𝒪.
        Store results: OPEX, CAPEX, Power Split, Battery Size, etc.
    end for
end for
Perform financial analysis: Compute Payback Period and ROI.
```

4.2. Case and scenario generation

In this work, a *case* is defined as a set of distinct scenarios of operation, where a *scenario* refers to a specific combination of the vessel's operational profile and the corresponding fuel price during that profile. Ideally, scenario and case generation would be based on a probability distribution function representing the likelihood of an event occurring. However, this information is considered proprietary and strategically sensitive. Therefore, a set of cases is developed to address the research objectives posed in Section 1.

Fig. 1 presents the probability density function of fuel prices based on historical data collected between 07/03/22 and 05/03/25, retrieved from [9]. The histogram is segmented using percentile-based thresholds to define representative fuel price levels. For example, dividing the distribution at the 33.3% and 66.67% percentiles yields three segments, whereas a 75% threshold results in two. Median values are sampled from within each segment to serve as representative fuel prices

Table 1
Median fuel price (C^{Fuel}) values in €-ton.

Percentile	0–33.3%	33.3–66.67%	66.67%–100%
C^{Fuel}	679	792	1059
Percentile	0–75%		75%–100%
C^{Fuel}	759		1114
Percentile	0–100%		
C^{Fuel}	792		

in the scenario generation process, alongside the overall median, as summarized in Table 1.

To balance representativeness and computational tractability, the 75% percentile split is selected as the primary basis for scenario definition. However, the full 0%–100% percentile range is also considered in select cases to assess sensitivity in energy storage requirements and scheduling outcomes under broader fuel price variability.

Three different operational profiles are considered, as shown in Figs. 3(a)–3(c). The percentage of time a specific load profile occurs is denoted by $\mathcal{L}_i$, where i represents the load profile number. The operational time during which the vessel is at port or not engaged in dredging operations (load profile 3) is assumed to be 100 days per year. Therefore, the corresponding value for $\mathcal{L}_3 = 100/365$

However, the percentage of time the vessel operates under load profiles 1 and 2 is uncertain. Three different possibilities are considered:

1. The vessel spends 25% of the remaining time in load profile 1 and 75% in load profile 2.
2. The vessel spends 75% of the remaining time in load profile 1 and 25% in load profile 2.
3. The vessel splits the remaining time equally between load profiles 1 and 2.

The split between load profile 1 and load profile 2 is represented by ω_1 and ω_2, respectively. The percentage of time spent in load profiles 1 and 2 is calculated as:

$$\mathcal{L}_i = \omega_i \cdot (1 - \mathcal{L}_3), \quad i = 1, 2 \tag{1}$$

With three load profiles and two different fuel prices, a total of six scenarios (denoted by $S_{i,j}$) are formed—i.e., two fuel price conditions $j \in [1, 2]$ for each of the three load profiles. Since there are three different possibilities for ω_i, this results in three distinct cases.

Similarly, in the case where a single fuel price is considered across all operational profiles, three scenarios are present—each scenario corresponding to one of the three load profiles but under the same fuel price. Again, with three configurations of ω_i, this yields three additional cases. A total of six cases are defined in the study:

- **Cases 1–3**: Each case includes **six scenarios**, constructed from all possible combinations of three operational load profiles and two distinct fuel price levels.
- **Cases 4–6**: Each case includes **three scenarios**, corresponding to the three load profiles evaluated under a *single*, fixed fuel price condition.

For cases 1–3, two different fuel costs are considered: C_1^{Fuel} and C_2^{Fuel}, and λ_1 and λ_2 denote the probabilities associated with the median fuel prices in two different segments of the fuel price distribution. As discussed earlier, when using a two-segment approach based on percentiles, the fuel price distribution is split at the 75% percentile. Therefore, C_1^{Fuel} corresponds to the median fuel price in the first segment (i.e., from 0% to 75%), where $\lambda_1 = 0.75$. Similarly, C_1^{Fuel} corresponds to the second segment (i.e., from 75% to 100%), where $\lambda_2 = 0.25$.

For cases 4–6, with one fuel cost are considered: C_1^{Fuel} where λ_1 denotes the probabilities associated with the median fuel prices in one different segment of the fuel price distribution. Therefore, C_1^{Fuel} corresponds to the median fuel price of the entire distribution (i.e., from

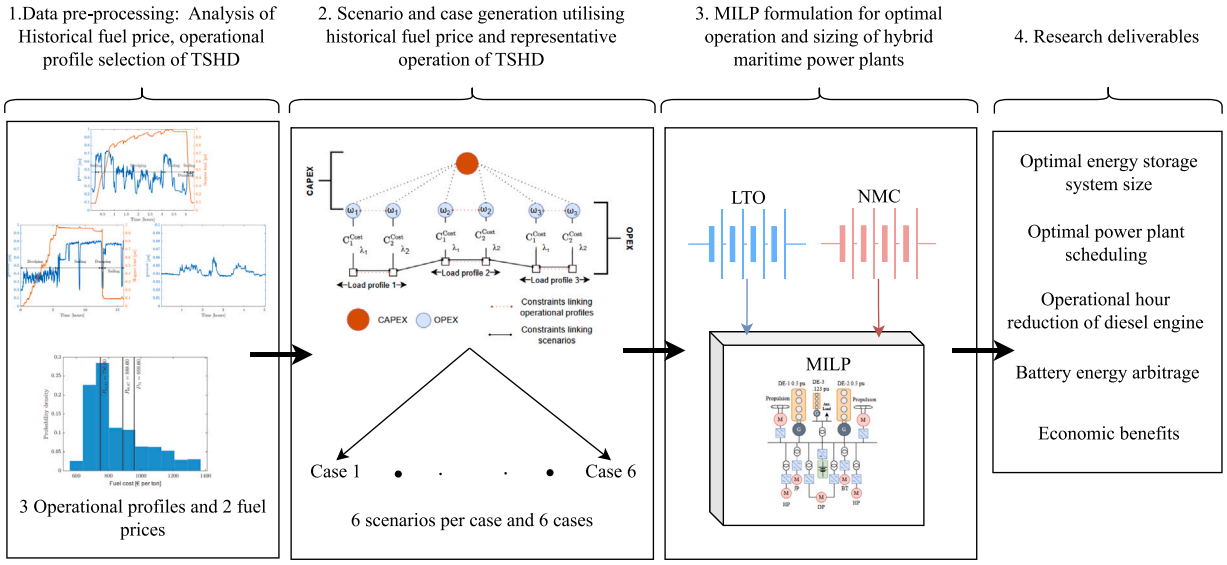

Fig. 6. 4-step methodology.

Table 2
Cases and Scenarios for dual fuel price (1–3). Where ω_i, λ_j represent the probability of load profile (i) and fuel price (j) occurrence.

Case	1	2	3
ω_1 / ω_2	0.25 / 0.75	0.75 / 0.25	0.5 / 0.5
λ_1	0.75	0.75	0.75
λ_2	0.25	0.25	0.25

Table 3
Cases and Scenarios for single fuel price (4–6). Where ω_i, λ_j represent the probability of load profile (i) and fuel price (j) occurrence.

Case	4	5	6
ω_1 / ω_2	0.75 / 0.25	0.25 / 0.75	0.5 / 0.5
λ_1	1	1	1
λ_2	0	0	0

0% to 100%), where $\lambda_1 = 1$. In this case, C_2^{Fuel} and λ_2 can be considered to be 0.

A detailed structure of the scenario tree is presented in Fig. 7 and the considered values of ω_i and λ_j are shown. The probability that a specific scenario $S_{i,j}$ occurs in a case is given by:

$$P(S_{i,j}) = \mathcal{L}_i \cdot \lambda_j, \text{where} \quad i \in \{1,2,3\}, \quad j \in \{1,2\} \tag{2}$$

The values for $P(S_{i,j})$ associated with different cases can be found in Table A.1. Given the limited number of scenarios, the two-stage stochastic problem can be reformulated as its deterministic equivalent and solved accordingly.

5. Mathematical model

This section presents the mathematical formulation of the hybrid power and energy management optimization problem. The model integrates component-level operational constraints, scenario-based uncertainty, and techno-economic metrics into a unified framework. All constants used throughout the formulation are summarized in Table 4, while the decision variables – both continuous and binary – are listed in Table 5. To enhance readability, constants are represented in standard font, whereas decision variables are highlighted in bold. The optimization framework captures load balancing, generator logic, battery dynamics, and financial performance under multiple operational scenarios, as described in subsequent subsections.

5.1. Objective function

The objective function ($\mathcal{O}$) is listed in Eq. (3). Here, $\mathbf{F}^{cost}_{S_{i,j}}$ is the fuel cost associated with scenario $S_{i,j}$ for load profile i and fuel price j. Similarly, $\mathbf{M}^{cost}_{S_{i,j}}$ represents the maintenance costs, and $\mathbf{B}^{cost}$ represents the capital investment required to install the battery system. The expected battery lifetime is denoted by T^{bat}_{life}, and the duration of each load profile is represented as $T^{profile}_i$.

The fuel consumption is calculated as shown in Eq. (3b), where $\mathbf{P}^{DE}_{S_{i,j},k}(t)$ is the power produced by the kth DE at time t. The operational status of the individual DE is given by the binary decision variable $\mathbf{U}^{DE}_{S_{i,j},k}(t)$. The cost of fuel is denoted by C^{Fuel}_j. The SFOC coefficients are denoted by α_k and β_k. The summation is taken over $t = 1, \ldots, T_{i,j}$, where T_i represents the total number of time steps in scenario $S_{i,j}$.

The maintenance cost associated with the operational hours of the DE is computed as per Eq. (3c). The maintenance cost per hour of the DE is denoted by C^{maint}_k.

Finally, the cost of installing a battery onboard is calculated using Eq. (3d), where $\mathbf{S}^{Bat}$ is the size of the battery and C_{bat} is the cost per kWh of battery capacity. The cost of the inverter per kW is denoted by C^{inv} and the minimum continuous discharge power per kWh of energy that the battery can produce is denoted by $P^{\frac{P}{E}}_{dch}$.

The scenario probabilities $P(S_{i,j})$ account for both the time spent at a particular operational profile and the fuel price occurrence. The total scenario probability is normalized such that the sum over all combinations equals 1.

$$\min \mathcal{O} = \underbrace{\mathbf{B}^{cost}}_{\text{CAPEX}} + \underbrace{\left(\sum_{i=1}^{3}\sum_{j=1}^{2}\left(\mathbf{F}^{cost}_{S_{i,j}} + \mathbf{M}^{cost}_{S_{i,j}}\right) \cdot P(S_{i,j}) \cdot \frac{T^{bat}_{life}}{T^{profile}_i}\right)}_{\text{OPEX}}, \quad \forall i,j \tag{3a}$$

$$F^{cost}_{S_{i,j}} = \sum_{k=1}^{3}\sum_{t=1}^{T_i}\left(\mathbf{P}^{DE}_{S_{i,j},k}(t) \cdot \alpha + \beta \cdot \mathbf{U}^{DE}_{S_{i,j},k}(t)\right) \cdot C^{Fuel}_j \, \Delta t, \quad \forall i,j \tag{3b}$$

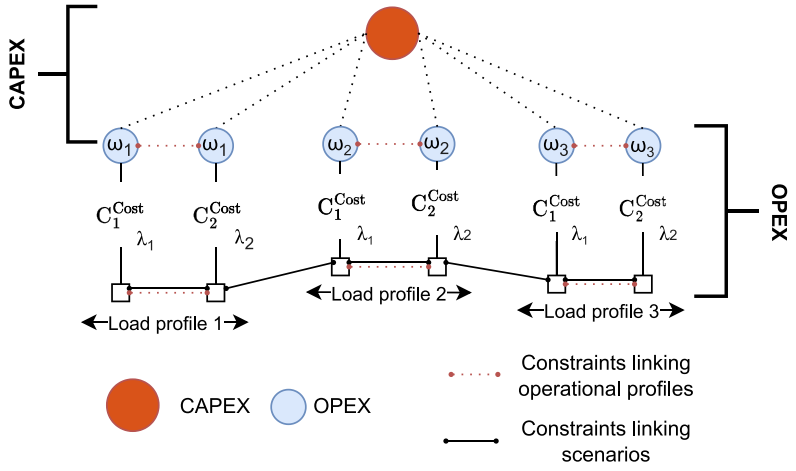

Fig. 7. Scenario tree of optimization model.

Table 4
Model constants and notation used in the optimization.

Symbol	Unit	Description	Value or Reference
i	–	Load profile index	$[1,2,3]$
j	–	Fuel price index	$[1,2]$
k	–	DE index	$[1,2,3]$
t	–	Time step index	$[1,2,\ldots,T_i]$
T_i	–	Number of time steps in load profile i	$[1103, 259, 600]$
$S_{i,j}$	–	Scenario formed by load profile i and fuel price j	Fig. 7 and Tables 2 and 3
$P(S_{i,j})$	–	Probability of scenario	Table A.1
ω_i	–	Fraction of remaining time assigned to load profile i	Tables 2 and 3
$\mathcal{L}_i$	–	Load profile time percentage	Eq. (1)
$\mathcal{L}_3$	–	Time spent in port profile (load profile 3)	$100/365 \approx 0.274$
λ_j	–	Fuel price scenario probability	Tables 2 and 3
T_{life}^{bat}	year	Battery lifetime	10
$T_i^{profile}$	year	Duration of load profile i	$[T_i] \cdot 365^{-1}$
C_j^{Fuel}	€/ton	Fuel cost per scenario	Table 1
$[\alpha_k, \beta_k]$	[ton/kWh, ton]	Fuel model coefficients	$[0.1822, 30.8397] \cdot 10^{-3}, \quad k \in [1,2]$
$[\alpha_3, \beta_3]$	[ton/kWh, ton]	Fuel model coefficients	$[0.1971, 16.482] \cdot 10^{-3} \quad k = 3$
C^{Maint}	€/h	DE maintenance cost per hour [DE1,2, AUX DE]	$[30, 7.25]$
C^{bat}	€/kWh	Battery system cost [LTO,NMC]	$[930, 500]$
C^{inv}	€/kW	Inverter cost	60 [37]
η_i	–	Inverter loss	2.5%, $\quad i \in [1,2]$, [16]
η_i	–	Inverter loss	5%, $\quad i = 3$
P_i^{demand}	kW	Power demand for load profile i	Figs. 3(a)–3(c)
BigM	–	Big-M constant for logic constraints	8000
P^R	kW	Required reserve power	8000
$P_{dch}^{\frac{p}{E}}$	h^{-1}	Continuous discharge power per kWh	$[3.75, 2.35]$ [10]
$P_{ch}^{\frac{p}{E}}$	h^{-1}	Continuous charge power per kWh	$[4.21, 0.93]$ [10]
T_{ON}^{min}	h	Minimum DE ON time	0.5
T_{OFF}^{min}	h	Minimum DE OFF time	0.5
P_{min}^{DE}	kW	Minimum DE power output	100
P_{max}^{DE}	kW	Maximum DE power output	4000
ΔP_{max}^{DE}	kW/min	Maximum DE ramp rate	2000
N^{cycles}	–	Battery lifetime in cycles [LTO,NMC]	$[20\,000, 7000]$
Savings	€	Total savings over benchmark scenario	Defined in Eq. (18a)
T_{PB}	years	Payback time	Defined in Eq. (18b)
ROI	–	Return on Investment	Defined in Eq. (18c)

Table 5
Decision variables.

Decision variables	Unit	Description
Continuous		
$\mathbf{B}^{\text{Cost}}$	€	Battery system cost
$\mathbf{F}^{\text{Cost}}_{S_{i,j}}$	€	Fuel cost
$\mathbf{M}^{\text{Cost}}_{S_{i,j}}$	€	Maintenance cost
$\mathbf{P}^{\text{DE}}_{S_{i,j,k}}(\mathbf{t})$	kW	DE power
$\mathbf{S}^{\text{Bat}}$	kWh	Battery size
$\mathbf{P}^{\text{bat}}_{S_{i,j}}(t)$	kW	Net battery power
$\mathbf{P}^{\text{dch}}_{S_{i,j}}(t)$	kW	Battery discharge power
$\mathbf{P}^{\text{ch}}_{S_{i,j}}(t)$	kW	Battery charge power
$\Delta\mathbf{P}^{\text{DE}}_{S_{i,j,k}}(t)$	kW	Ramp rate of DE
$\mathbf{T}^{\text{DE}_{\text{ON}}}_{S_{i,j,k}}(t)$	Δt	DE ON time counter
$\mathbf{T}^{\text{DE}_{\text{OFF}}}_{S_{i,j,k}}(t)$	Δt	DE OFF time counter
$\mathbf{E}^{\text{bat}}_{S_{i,j}}(t)$	kWh	Energy in battery
Binary		
$\mathbf{U}^{\text{DE}}_{S_{i,j,k}}(t)$, $\bar{\mathbf{U}}^{\text{DE}}_{S_{i,j,k}}(t)$	–	DE status (ON/OFF)
$\mathbf{U}^{\text{DE}_{\text{ON}}}_{S_{i,j,k}}(t)$	–	Marks last time step the DE was ON
$\mathbf{U}^{\text{DE}_{\text{OFF}}}_{S_{i,j,k}}(t)$	–	Marks last time step the DE was OFF
$\mathbf{U}^{\text{dch}}_{S_{i,j}}(t)$	–	Battery discharge status
$\mathbf{U}^{\text{ch}}_{S_{i,j}}(t)$	–	Battery charging status

$$\mathrm{M}^{\text{cost}}_{S_{i,j}} = \sum_{k=1}^{3}\sum_{t=1}^{T_i} \mathbf{U}^{\mathbf{DE}}_{\mathbf{S_{i,j,k}}}(\mathbf{t}) \cdot \mathrm{C}^{\text{maint}}_{k}\,\Delta t, \quad \forall i,j \tag{3c}$$

$$\mathrm{B}^{\text{cost}} = \mathbf{S}^{\text{Bat}} \cdot \mathrm{C}_{\text{bat}} + \mathbf{S}^{\text{Bat}} \cdot \mathrm{P}^{\frac{\mathrm{P}}{\mathrm{E}}}_{\text{dch}} \cdot \mathrm{C}^{\text{inv}} \tag{3d}$$

5.2. Load balance

The power system's load balance equation is given in Eq. (4). In this equation, $\mathbf{P}^{\text{bat}}_{S_{i,j}}(\mathbf{t})$ represents the power delivered by the battery, while $\mathrm{P}^{\text{demand}}_{i}$ denotes the total power demand, including both propulsion power and electrical loads. The charging and discharging efficiency is represented by η, whereas the magnitudes of the charging and discharging power are given by $\mathbf{P}^{\text{ch}}_{S_{i,j}}(\mathbf{t})$ and $\mathbf{P}^{\text{dch}}_{S_{i,j}}(\mathbf{t})$, respectively.

$$\sum_{k=1}^{3} \mathbf{P}^{\mathbf{DE}}_{\mathbf{S_{i,j,k}}}(\mathbf{t}) + \mathbf{P}^{\mathbf{bat}}_{\mathbf{S_{i,j}}}(\mathbf{t}) = \mathrm{P}^{\text{demand}}_{i} + \eta \cdot \left(\mathbf{P}^{\mathbf{dch}}_{\mathbf{S_{i,j}}}(\mathbf{t}) + \mathbf{P}^{\mathbf{ch}}_{\mathbf{S_{i,j}}}(\mathbf{t})\right), \quad \forall i,j,t \tag{4}$$

5.3. Diesel engine

The DE can generate power within a specified range, constrained by a minimum and maximum power limit, as represented in (5). Here, $\mathrm{P}^{\text{DE}}_{k-\min}$ and $\mathrm{P}^{\text{DE}}_{k-\max}$ denote the minimum and maximum power output of the DE when it is operating. The binary variable $\mathbf{U}^{\mathbf{DE}}_{\mathbf{S_{i,j,k}}}(\mathbf{t})$ determines whether the kth DE is active in scenario $S_{i,j}$ at time t, and $\mathbf{P}^{\mathbf{DE}}_{\mathbf{S_{i,j,k}}}(\mathbf{t})$ represents its corresponding power output.

$$\mathbf{U}^{\mathbf{DE}}_{\mathbf{S_{i,j,k}}}(\mathbf{t}) \cdot \mathrm{P}^{\text{DE}}_{k-\min} \le \mathbf{P}^{\mathbf{DE}}_{\mathbf{S_{i,j,k}}}(\mathbf{t}) \le \mathbf{U}^{\mathbf{DE}}_{\mathbf{S_{i,j,k}}}(\mathbf{t}) \cdot \mathrm{P}^{\text{DE}}_{k-\max}, \quad \forall i,j,k,t \tag{5}$$

The AUX DE is turned OFF during load profiles 1 and 2, while both DE-1 and DE-2 are turned OFF during load profile 3. These constraints are shown in Eq. (6).

$$\mathbf{U}^{\mathbf{DE}}_{\mathbf{S_{i,j,3}}} = 0 \quad \forall i,j \in [1,2] \tag{6a}$$

$$\mathbf{U}^{\mathbf{DE}}_{\mathbf{S_{3,j,k}}} = 0 \quad \forall j,k \in [1,2] \tag{6b}$$

The DE cannot be turned ON and OFF repeatedly due to operational constraints and the fuel consumed during start-up. These operational limitations are modeled using the Big M integer method, as shown in Eq. Eq. (7). The decision variable $\mathbf{T}^{\mathbf{DE_{ON}}}_{\mathbf{S_{i,j,k}}}(\mathbf{t})$ is introduced to track the duration for which the kth DE has been continuously operating in scenario $S_{i,j}$. The Big M integer is denoted by BigM. If the DE is ON, the value of $\mathbf{T}^{\mathbf{DE_{ON}}}_{\mathbf{S_{i,j,k}}}(\mathbf{t})$ is incremented by 1 during each time step.

$$\mathbf{T}^{\mathbf{DE_{ON}}}_{\mathbf{S_{i,j,k}}}(\mathbf{t}) \le \mathbf{T}^{\mathbf{DE_{ON}}}_{\mathbf{S_{i,j,k}}}(\mathbf{t-1}) + 1 + \text{BigM} \cdot \left(1 - \mathbf{U}^{\mathbf{DE}}_{\mathbf{S_{i,j,k}}}(\mathbf{t})\right), \quad \forall i,j,k,\ t \ne 1, \tag{7a}$$

$$\mathbf{T}^{\mathbf{DE_{ON}}}_{\mathbf{S_{i,j,k}}}(\mathbf{t}) \ge \mathbf{T}^{\mathbf{DE_{ON}}}_{\mathbf{S_{i,j,k}}}(\mathbf{t-1}) + 1 - \text{BigM} \cdot \left(1 - \mathbf{U}^{\mathbf{DE}}_{\mathbf{S_{i,j,k}}}(\mathbf{t})\right), \quad \forall i,j,k,\ t \ne 1, \tag{7b}$$

$$\mathbf{T}^{\mathbf{DE_{ON}}}_{\mathbf{S_{i,j,k}}}(\mathbf{t}) \le \text{BigM} \cdot \mathbf{U}^{\mathbf{DE}}_{\mathbf{S_{i,j,k}}}(\mathbf{t}), \quad \forall i,j,k,\ t \ne 1, \tag{7c}$$

$$\mathbf{T}^{\mathbf{DE_{ON}}}_{\mathbf{S_{i,j,k}}}(\mathbf{t}) \ge -\text{BigM} \cdot \mathbf{U}^{\mathbf{DE}}_{\mathbf{S_{i,j,k}}}(\mathbf{t}), \quad \forall i,j,k,\ t \ne 1. \tag{7d}$$

To ensure that the DE remains ON for a minimum duration ($\mathrm{T}^{\min}_{\text{ON}}$), a binary decision variable $\mathbf{U}^{\mathbf{DE_{ON}}}_{\mathbf{S_{i,j,k}}}(\mathbf{t})$ is introduced to identify the final time step at which the kth DE is ON in scenario $S_{i,j}$, as modeled in Eq. (8). Furthermore, when $\mathbf{U}^{\mathbf{DE_{ON}}}_{\mathbf{S_{i,j,k}}}(\mathbf{t})$ equals 1, Eq. (8d) ensures that the continuous variable $\mathbf{T}^{\mathbf{DE_{ON}}}_{\mathbf{S_{i,j,k}}}(\mathbf{t})$ is greater than or equal to the minimum ON time $\mathrm{T}^{\min}_{\text{ON}}$.

$$\mathbf{U}^{\mathbf{DE}}_{\mathbf{S_{i,j,k}}}(\mathbf{t-1}) - \mathbf{U}^{\mathbf{DE}}_{\mathbf{S_{i,j,k}}}(\mathbf{t}) \le \mathbf{U}^{\mathbf{DE_{ON}}}_{\mathbf{S_{i,j,k}}}(\mathbf{t-1}), \quad \forall i,j,k,\ t \ne 1, \tag{8a}$$

$$1 - \mathbf{U}^{\mathbf{DE}}_{\mathbf{S_{i,j,k}}}(\mathbf{t}) \ge \mathbf{U}^{\mathbf{DE_{ON}}}_{\mathbf{S_{i,j,k}}}(\mathbf{t-1}), \quad \forall i,j,k,\ t \ne 1, \tag{8b}$$

$$\mathbf{U}^{\mathbf{DE}}_{\mathbf{S_{i,j,k}}}(\mathbf{t-1}) \ge \mathbf{U}^{\mathbf{DE_{ON}}}_{\mathbf{S_{i,j,k}}}(\mathbf{t-1}), \quad \forall i,j,k,\ t \ne 1, \tag{8c}$$

$$\mathbf{T}^{\mathbf{DE_{ON}}}_{\mathbf{S_{i,j,k}}}(\mathbf{t}) \ge \mathrm{T}^{\min}_{\text{ON}} - \text{BigM} \cdot \left(1 - \mathbf{U}^{\mathbf{DE_{ON}}}_{\mathbf{S_{i,j,k}}}(\mathbf{t})\right), \quad \forall i,j,k,\ t \tag{8d}$$

Similarly, a minimum OFF time ($\mathrm{T}^{\min}_{\text{OFF}}$) is enforced using equation Eq. (9). A continuous decision variable, $\mathbf{T}^{\mathbf{DE_{OFF}}}_{\mathbf{S_{i,j,k}}}(\mathbf{t})$, is introduced to track the OFF time, analogous to $\mathbf{T}^{\mathbf{DE_{ON}}}_{\mathbf{S_{i,j,k}}}(\mathbf{t})$, as shown in Eq. (9). This decision variable increments by 1 at each time step when the DE is OFF. The OFF status of the DE is modeled using a binary decision variable, $\bar{\mathbf{U}}^{\mathbf{DE}}_{\mathbf{S_{i,j,k}}}(\mathbf{t})$, which takes the value 1 when the DE is OFF, as defined in Eq. (10).

$$\mathbf{T}^{\mathbf{DE_{OFF}}}_{\mathbf{S_{i,j,k}}}(\mathbf{t}) \le \mathbf{T}^{\mathbf{DE_{OFF}}}_{\mathbf{S_{i,j,k}}}(\mathbf{t-1}) + 1 + \text{BigM} \cdot \left(1 - \bar{\mathbf{U}}^{\mathbf{DE}}_{\mathbf{S_{i,j,k}}}(\mathbf{t})\right), \quad \forall i,j,k,\ t \ne 1, \tag{9a}$$

$$\mathbf{T}^{\mathbf{DE_{OFF}}}_{\mathbf{S_{i,j,k}}}(\mathbf{t}) \ge \mathbf{T}^{\mathbf{DE_{OFF}}}_{\mathbf{S_{i,j,k}}}(\mathbf{t-1}) + 1 - \text{BigM} \cdot \left(1 - \bar{\mathbf{U}}^{\mathbf{DE}}_{\mathbf{S_{i,j,k}}}(\mathbf{t})\right), \quad \forall i,j,k,\ t \ne 1, \tag{9b}$$

$$\mathbf{T}^{\mathbf{DE_{OFF}}}_{\mathbf{S_{i,j,k}}}(\mathbf{t}) \le \text{BigM} \cdot \bar{\mathbf{U}}^{\mathbf{DE}}_{\mathbf{S_{i,j,k}}}(\mathbf{t}), \quad \forall i,j,k,\ t, \tag{9c}$$

$$\mathbf{T}^{\mathbf{DE_{OFF}}}_{\mathbf{S_{i,j,k}}}(\mathbf{t}) \ge -\text{BigM} \cdot \bar{\mathbf{U}}^{\mathbf{DE}}_{\mathbf{S_{i,j,k}}}(\mathbf{t}), \quad \forall i,j,k,\ t. \tag{9d}$$

$$\bar{\mathbf{U}}^{\mathbf{DE}}_{\mathbf{S_{i,j,k}}}(\mathbf{t}) + \mathbf{U}^{\mathbf{DE}}_{\mathbf{S_{i,j,k}}}(\mathbf{t}) = 1, \quad \forall i,j,k,t. \tag{10}$$

Eq. (11) is analogous to Eq. (8), but it ensures that the DE remains OFF for at least a duration of $\mathrm{T}^{\min}_{\text{OFF}}$. To enforce this constraint, a binary decision variable $\mathbf{U}^{\mathbf{DE_{OFF}}}_{\mathbf{S_{i,j,k}}}(\mathbf{t})$ is introduced to identify the last time step when the kth DE was OFF before being switched ON again in scenario

$S_{i,j}$. This guarantees that the continuous decision variable $\mathbf{T}^{\mathbf{DE_{OFF}}}_{S_{\mathbf{i,j}},\mathbf{k}}(\mathbf{t})$ in Eq. (11d) is greater than or equal to $\mathrm{T}^{\min}_{\mathrm{OFF}}$ whenever $\mathbf{U}^{\mathbf{DE_{OFF}}}_{S_{\mathbf{i,j}},\mathbf{k}}(\mathbf{t}) = 1$.

$$\bar{\mathbf{U}}^{\mathbf{DE}}_{S_{\mathbf{i,j}},\mathbf{k}}(\mathbf{t-1}) - \bar{\mathbf{U}}^{\mathbf{DE}}_{S_{\mathbf{i,j}},\mathbf{k(t)}} \leq \mathbf{U}^{\mathbf{DE_{OFF}}}_{S_{\mathbf{i,j}},\mathbf{k}}(\mathbf{t-1}), \quad \forall i,j,k,t \neq 1, \tag{11a}$$

$$1 - \bar{\mathbf{U}}^{\mathbf{DE}}_{S_{\mathbf{i,j}},\mathbf{k}}(\mathbf{t}) \geq \mathbf{U}^{\mathbf{DE_{OFF}}}{}_{S_{\mathbf{i,j}},\mathbf{k}}(\mathbf{t-1}), \quad \forall i,j,k,t \neq 1, \tag{11b}$$

$$\bar{\mathbf{U}}^{\mathbf{DE}}_{S_{\mathbf{i,j}},\mathbf{k}}(\mathbf{t-1}) \geq \mathbf{U}^{\mathbf{DE_{OFF}}}{}_{S_{\mathbf{i,j}},\mathbf{k}}(\mathbf{t-1}), \quad \forall i,j,k,t \neq 1, \tag{11c}$$

$$\mathbf{T}^{\mathbf{DE_{OFF}}}_{S_{\mathbf{i,j}},\mathbf{k}}(\mathbf{t}) \geq \mathrm{T}^{\min}_{\mathrm{OFF}} - \mathrm{BigM}\cdot\left(1 - \bar{\mathbf{U}}^{\mathbf{DE}}_{S_{\mathbf{i,j}},\mathbf{k}}(\mathbf{t-1})\right), \quad \forall i,j,k,t \neq 1. \tag{11d}$$

When two DE generator sets operate simultaneously and are connected to the same AC bus, they function in parallel, sharing the load according to their capacity. For equally sized DEs, the load is distributed equally. This behavior is modeled in Eq. (12). In this formulation, Eq. (12a) ensures that DE-1 is prioritized to be ON before DE-2 in each scenario $S_{i,j}$. This simplification facilitates modeling of parallel loading conditions, where Eqs. (12b)–(12d) ensure that if DE-2 is ON, the load is equally distributed between both DEs.

$$\mathbf{U}^{\mathbf{DE}}_{S_{\mathbf{i,j}},\mathbf{1}}(\mathbf{t}) \geq \mathbf{U}^{\mathbf{DE}}_{S_{\mathbf{i,j}},\mathbf{2}}(\mathbf{t}), \quad \forall i,j,t, \tag{12a}$$

$$\mathbf{P}^{\mathbf{DE}}_{S_{\mathbf{i,j}},\mathbf{2}}(\mathbf{t}) \geq \mathrm{BigM}\cdot\mathbf{U}^{\mathbf{DE}}_{S_{\mathbf{i,j}},\mathbf{2}}(\mathbf{t}), \quad \forall i,j,t, \tag{12b}$$

$$\mathbf{P}^{\mathbf{DE}}_{S_{\mathbf{i,j}},\mathbf{2}}(\mathbf{t}) \geq \mathbf{P}^{\mathbf{DE}}_{S_{\mathbf{i,j}},\mathbf{1}}(\mathbf{t}) - \mathrm{BigM}\cdot\left(1 - \mathbf{U}^{\mathbf{DE}}_{S_{\mathbf{i,j}},\mathbf{2}}(\mathbf{t})\right), \quad \forall i,j,t, \tag{12c}$$

$$\mathbf{P}^{\mathbf{DE}}_{S_{\mathbf{i,j}},\mathbf{1}}(\mathbf{t}) \geq \mathbf{P}^{\mathbf{DE}}_{S_{\mathbf{i,j}},\mathbf{2}}(\mathbf{t}), \quad \forall i,j,t. \tag{12d}$$

The ramp rates of the DEs are captured by the decision variable $\mathbf{\Delta P}^{\mathbf{DE}}_{S_{\mathbf{i,j}},\mathbf{k}}(\mathbf{t})$, as defined in Eq. (13). Once the solution to the objective function in Eq. (3a) is obtained, $\mathbf{\Delta P}^{\mathbf{DE}}_{S_{\mathbf{i,j}},\mathbf{k}}(\mathbf{t})$ is minimized in a secondary optimization step, while keeping the solution of Eq. (3a) and the decision variable $\mathbf{S}^{\mathrm{Bat}}$ fixed as constraints. This approach ensures a reasonable power split without altering the previously obtained solution. Additionally, Eq. (13c) enforces the ramping limits of the DE, where $\Delta\mathrm{P}^{\mathrm{DE}}_{\max}$ represents the maximum allowable power ramp for each DE at each time step.

$$\mathbf{\Delta P}^{\mathbf{DE}}_{S_{\mathbf{i,j}},\mathbf{k}}(\mathbf{t}) \geq \mathbf{P}^{\mathbf{DE}}_{S_{\mathbf{i,j}},\mathbf{k}}(\mathbf{t}) - \mathbf{P}^{\mathbf{DE}}_{S_{\mathbf{i,j}},\mathbf{k}}(\mathbf{t-1}), \quad \forall i,j,k,t \neq 1, \tag{13a}$$

$$\mathbf{\Delta P}^{\mathbf{DE}}_{S_{\mathbf{i,j}},\mathbf{k}}(\mathbf{t}) \geq \mathbf{P}^{\mathbf{DE}}_{S_{\mathbf{i,j}},\mathbf{k}}(\mathbf{t-1}) - \mathbf{P}^{\mathbf{DE}}_{S_{\mathbf{i,j}},\mathbf{k}}(\mathbf{t}), \quad \forall i,j,k,t \neq 1, \tag{13b}$$

$$\mathbf{\Delta P}^{\mathbf{DE}}_{S_{\mathbf{i,j}},\mathbf{k}}(\mathbf{t}) \leq \Delta\mathrm{P}^{\mathrm{DE}}_{\max}, \quad \forall i,j,k,t \neq 1. \tag{13c}$$

Turning off a DE implies that the available power onboard to compensate for sudden changes in load is reduced, and system redundancy is also decreased. To address this, a power reserve constraint is introduced in Eq. (14). This constraint ensures that a minimum of 8000 kW is available in the system at all times whenever a battery is added to facilitate the shutdown of a DE.

$$\mathrm{P}^{\mathrm{R}}_{\mathbf{i,j}} \geq \sum_{k=1}^{2} \mathbf{U}^{\mathbf{DE}}_{S_{\mathbf{i,j}},\mathbf{k}}(\mathbf{t})\cdot\mathrm{P}^{\mathrm{DE}}_{\max} + \mathbf{S}^{\mathrm{Bat}}\cdot\mathrm{P}^{\frac{\mathrm{P}}{\mathrm{E}}}_{\mathrm{dch}}, \quad \forall i\in[1,2],j,t \tag{14}$$

5.4. Battery

The energy stored in the battery is represented by the decision variable $\mathbf{E}^{\mathrm{bat}}_{S_{\mathbf{i,j}}}(\mathbf{t})$. The battery's energy is modeled in Eq. (15a). Fig. 7 illustrates the linking constraints between different scenarios within an operational profile. Specifically, Eqs. (15b) and (15c) enforce a linking constraint to ensure that the energy stored in the battery at the end of each load profile is equal to the energy available at the beginning of the load profile. The energy management system must also ensure that the battery is not fully charged or discharged. This is achieved by constraining the battery's state of energy between 10% and 90% of its total capacity, as shown in Eq. (15d). The battery system is also limited by a maximum continuous power for both charging and discharging. Typically, this limit is defined by the battery's C-rate. However, since this energy and power model does not explicitly account for current and voltage, a charging power-to-energy ratio $\mathrm{P}^{\frac{\mathrm{P}}{\mathrm{E}}}_{\mathrm{ch}}$ and a discharging ratio $\mathrm{P}^{\frac{\mathrm{P}}{\mathrm{E}}}_{\mathrm{dch}}$ are introduced. These ratios define the maximum continuous charging and discharging power the battery can provide per unit of installed energy capacity.

$$\mathbf{E}^{\mathrm{bat}}_{S_{\mathbf{i,j}}}(\mathbf{t}) = \mathbf{E}^{\mathrm{bat}}_{S_{\mathbf{i,j}}}(\mathbf{t-1}) - \mathbf{P}^{\mathrm{bat}}_{S_{\mathbf{i,j}}}(\mathbf{t})\cdot\Delta t, \quad \forall i,j,t \neq 1, \tag{15a}$$

$$\mathbf{E}^{\mathrm{bat}}_{S_{\mathbf{i,j}}}(\mathbf{1}) = \mathbf{E}^{\mathrm{bat}}_{\mathbf{i}}(\mathbf{1}), \quad \forall i,j, \tag{15b}$$

$$\mathbf{E}^{\mathrm{bat}}_{S_{\mathbf{i,j}}}(\mathrm{T}^{\mathrm{profile}}_{\mathbf{i}}) = \mathbf{E}^{\mathrm{bat}}_{\mathbf{i}}(\mathrm{T}^{\mathrm{profile}}_{\mathbf{i}}), \quad \forall i,j, \tag{15c}$$

$$0.1\cdot\mathbf{S}^{\mathrm{Bat}} \leq \mathbf{E}^{\mathrm{bat}}_{S_{\mathbf{i,j}}}(\mathbf{t}) \leq 0.9\cdot\mathbf{S}^{\mathrm{Bat}}, \quad \forall i,j,t, \tag{15d}$$

$$-\mathbf{S}^{\mathrm{Bat}}\cdot\mathrm{P}^{\frac{\mathrm{P}}{\mathrm{E}}}_{\mathrm{ch}} \leq \mathbf{P}^{\mathrm{bat}}_{S_{\mathbf{i,j}}}(\mathbf{t}) \leq \mathbf{S}^{\mathrm{Bat}}\cdot\mathrm{P}^{\frac{\mathrm{P}}{\mathrm{E}}}_{\mathrm{dch}}, \quad \forall i,j,t. \tag{15e}$$

Fig. 7 illustrates the constraints linking different operational profiles. Such a constraint defines the maximum allowable battery throughput over its lifetime. This is modeled in Eq. (16), where the total battery throughput accounts for various operational profiles (i) and fuel price scenarios (j), indexed by scenario $S_{i,j}$. This linking constraint enables flexible battery usage across different load profiles and fuel price scenarios, allowing the battery to be utilized more intensively in certain periods if it is beneficial to the overall system performance.

$$\sum_{i=1}^{2}\sum_{j=1}^{3}\sum_{t=1}^{T_i}\mathbf{P}^{\mathrm{dch}}_{S_{i,j}}(t)\,\Delta t\cdot\frac{\sum_{i=1}^{2}\sum_{j=1}^{3}P(S_{i,j})\cdot\mathrm{T}^{\mathrm{profile}}_{i}}{\mathrm{T}^{\mathrm{bat}}_{\mathrm{life}}} \leq \mathbf{S}^{\mathrm{Bat}}\cdot\mathrm{N}^{\mathrm{cycles}} \tag{16a}$$

The discharge power $\mathbf{P}^{\mathrm{dch}}_{S_{\mathbf{i,j}}}$ and charging power $\mathbf{P}^{\mathrm{ch}}_{S_{\mathbf{i,j}}}$ of the battery, collectively represented as $\mathbf{P}^{\mathrm{bat}}_{S_{\mathbf{i,j}}}$, are determined according to Eq. (17). Eqs. (17a)–(17f) ensure that the decision variable $\mathbf{P}^{\mathrm{dch}}_{S_{\mathbf{i,j}}}$ captures only the positive portion of $\mathbf{P}^{\mathrm{bat}}_{S_{\mathbf{i,j}}}$, where $\mathbf{U}^{\mathrm{dch}}_{S_{\mathbf{i,j}}}$ is a binary decision variable set to 1 when the battery is discharging. Furthermore, Eq. (17g) ensures that the decision variable $\mathbf{P}^{\mathrm{ch}}_{S_{\mathbf{i,j}}}$ reflects the magnitude of the charging power.

$$\mathbf{P}^{\mathrm{bat}}_{S_{\mathbf{i,j}}}(\mathbf{t}) \geq -\mathrm{BigM}\cdot\left(1 - \mathbf{P}^{\mathrm{dch}}_{S_{\mathbf{i,j}}}(\mathbf{t})\right), \quad \forall i,j,t, \tag{17a}$$

$$\mathbf{P}^{\mathrm{bat}}_{S_{\mathbf{i,j}}}(\mathbf{t}) \leq \mathrm{BigM}\cdot\mathbf{P}^{\mathrm{dch}}_{S_{\mathbf{i,j}}}(\mathbf{t}), \quad \forall i,j,t, \tag{17b}$$

$$\mathbf{P}^{\mathrm{dch}}_{S_{\mathbf{i,j}}}(\mathbf{t}) \leq \mathbf{P}^{\mathrm{bat}}_{S_{\mathbf{i,j}}}(\mathbf{t}) + \mathrm{BigM}\cdot\left(1 - \mathbf{U}^{\mathrm{dch}}_{S_{\mathbf{i,j}}}(\mathbf{t})\right), \quad \forall i,j,t, \tag{17c}$$

$$\mathbf{P}^{\mathrm{dch}}_{S_{\mathbf{i,j}}}(\mathbf{t}) \geq \mathbf{P}^{\mathrm{bat}}_{S_{\mathbf{i,j}}}(\mathbf{t}) - \mathrm{BigM}\cdot\left(1 - \mathbf{U}^{\mathrm{dch}}_{S_{\mathbf{i,j}}}(\mathbf{t})\right), \quad \forall i,j,t, \tag{17d}$$

$$\mathbf{P}^{\mathrm{dch}}_{S_{\mathbf{i,j}}}(\mathbf{t}) \leq \mathrm{BigM}\cdot\mathbf{U}^{\mathrm{dch}}_{S_{\mathbf{i,j}}}(\mathbf{t}), \quad \forall i,j,t, \tag{17e}$$

$$\mathbf{P}^{\mathrm{dch}}_{S_{\mathbf{i,j}}}(\mathbf{t}) \geq -\mathrm{BigM}\cdot\mathbf{U}^{\mathrm{dch}}_{S_{\mathbf{i,j}}}(\mathbf{t}), \quad \forall i,j,t, \tag{17f}$$

$$\mathbf{P}^{\mathrm{ch}}_{S_{\mathbf{i,j}}}(\mathbf{t}) = \mathbf{P}^{\mathrm{dch}}_{S_{\mathbf{i,j}}}(\mathbf{t}) - \mathbf{P}^{\mathrm{bat}}_{S_{\mathbf{i,j}}}(\mathbf{t}), \quad \forall i,j,t. \tag{17g}$$

5.5. Financial calculations

The payback period for hybridizing the power plant refers to the amount of time required to recover the initial capital expenditure through annual fuel savings. Assuming the annual savings remain constant and interest rates are not considered, the payback period ($\mathrm{T_{PB}}$, in years) can be calculated as shown in Eq. (18b), where $\mathrm{F}^{\mathrm{benchmark}}_{S_{i,j}}$ represents the fuel consumption of the non-hybrid power plant, and $\mathrm{M}^{\mathrm{benchmark}}_{S_{i,j}}$ denotes the maintenance costs associated with a system without a battery. The ROI can be calculated as shown in Eq. (18c).

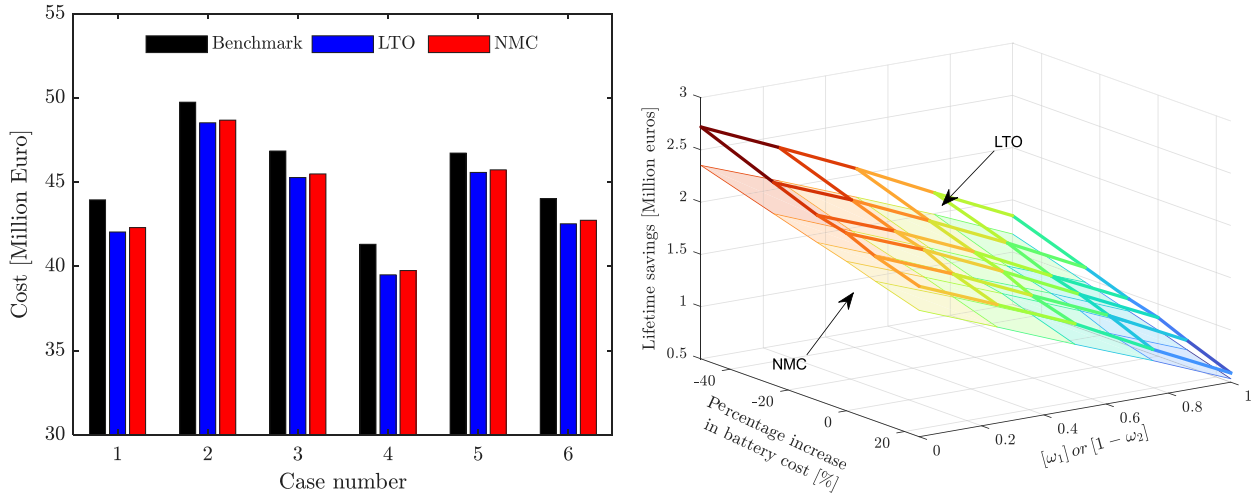

(a) Comparison of lifetime costs

(b) Sensitivity analysis of lifetime savings as a function of ω_1/ω_2 and battery cost

Fig. 8. Life time cost–benefit analysis of hybrid power plant.

Table 6
Necessary battery size (kWh) with relaxed reserve power constraints.

Battery	Case					
	1	2	3	4	5	6
LTO	510	487	487	498	487	487
NMC	215	892	569	217	215	215

$$\text{Savings} = \sum_{i=1}^{3}\sum_{j=1}^{2}\left(\mathbf{F}^{\mathbf{cost}}_{\mathbf{S_{i,j}}} + \mathbf{M}^{\mathbf{cost}}_{\mathbf{S_{i,j}}}\right) - \left(\sum_{i=1}^{3}\sum_{j=1}^{2} \mathrm{F}^{\text{benchmark}}_{S_{i,j}} + \mathrm{M}^{\text{benchmark}}_{S_{i,j}}\right) \tag{18a}$$

$$\mathrm{T_{PB}} = \frac{\mathbf{B^{cost}}}{\frac{\text{Savings}}{\mathrm{T^{bat}_{life}}}} \tag{18b}$$

$$\text{ROI} = \frac{(\text{Savings} - \mathbf{B^{cost}}) \cdot 100}{\mathbf{B^{cost}}} \tag{18c}$$

6. Results and discussion

This section presents and discusses the results. The financial implications of hybrid power plants are discussed in Section 6.1, while the operational strategies for the power plants are examined in Section 6.2.

6.1. Financial implications

The required battery sizes for LTO and NMC batteries remain constant across all cases (1–6) due to the reserve power constraint in Eq. (14). The battery capacities, rounded up to the nearest integer, are 1066 kWh for LTO and 1703 kWh for NMC. When the reserve power constraint is relaxed, the required battery size varies with operational time across different load profiles for both LTO and NMC chemistries. This variation is more prominent for NMC batteries, particularly when comparing different fuel price scenarios (i.e., cases 1–3 versus cases 4–6). The battery sizes for both chemistries across all six scenarios are presented in Table 6.

The rest of the study will focus on the results obtained with reserve power requirements. The corresponding lifetime cost (objective $\mathcal{O}$) for each case is presented in Fig. 8(a). The split in operational costs in depicted in Table A.2. Across all cases, hybrid power plants consistently result in lower lifetime costs compared to the benchmark case, regardless of battery type, fuel price, or operating scenario. Furthermore, hybrid systems integrated with LTO batteries always yield lower lifetime costs than those using NMC batteries. As expected, the lifetime cost is strongly influenced by the fuel price—this is evident when comparing cases 1–3 with cases 4–6. It is also affected by the proportion of time the vessel operates under load profiles 1 and 2, as seen when comparing cases 1–3 with each other and cases 4–6 with each other. The lifetime cost results are tabulated in Table A.3. Fig. 8(b) presents a sensitivity analysis showing that lifetime savings decrease as time spent in Load Profile 1 increases and time in Load Profile 2 decreases. This is attributed to the fact that, under Load Profile 2, DE-2 can remain off for extended periods compared to Load Profile 1, leading to increased maintenance savings. This effect is further elaborated in the remainder of the paper. Additionally, the sensitivity analysis evaluates potential lifetime savings as a function of the percentage increase in battery cost per kWh, over the range $[-50\%, 25\%]$. Lifetime savings remain positive even with a 25% increase in battery costs. Across the entire range, LTO batteries yield higher lifetime savings than NMC batteries. However, the difference between the two chemistries becomes negligible as ω_1 increases (or equivalently, as ω_2 decreases).

The battery system cost for LTO batteries ranges from 2.5–3% of the overall expenses (OPEX+CAPEX). Whereas for NMC batteries this ranges from 2.3–2.8% of the overall expenses. The overall expenses are dominated by the fuel costs that range from 91.4–92.4%. The detailed split of the lifetime costs are tabulated in Table A.4. The calculated payback time/period ($\mathrm{T_{PB}}$) in years as shown in Table A.5 is visually depicted in Fig. 9. The figure indicates the range of possible payback time and ROI incurred for different cases. The difference in payback period and ROI is comparatively insignificant between the two chemistries. Ranging from a payback period of 3.9 and 3.9 to 5.1 to 5.2 years for LTO and NMC batteries, respectively. Similarly, the possible return on investments ranges from 93.2% and 91.0% to 155% and 151%, respectively.

The cost of useful energy per euro is illustrated in Fig. 10. Fuel costs constitute the majority of the cost per kWh, while maintenance and CAPEX contribute significantly less, by approximately an order of magnitude. The total cost per kWh ranges from €0.1706–0.186 for the benchmark case, €0.166–0.178 for systems with LTO batteries, and €0.167–0.179 for systems with NMC batteries. For LTO batteries, the contributions of fuel, maintenance, and CAPEX to the total energy cost range from 91.3–92.3%, 5.0–5.4%, and 2.5–3%, respectively. In the case of NMC batteries, the corresponding ranges are 91.4–92.1% for fuel, 5.5–6% for maintenance, and 2.3–2.8% for CAPEX. The detailed contributions per case are depicted in Table A.6.

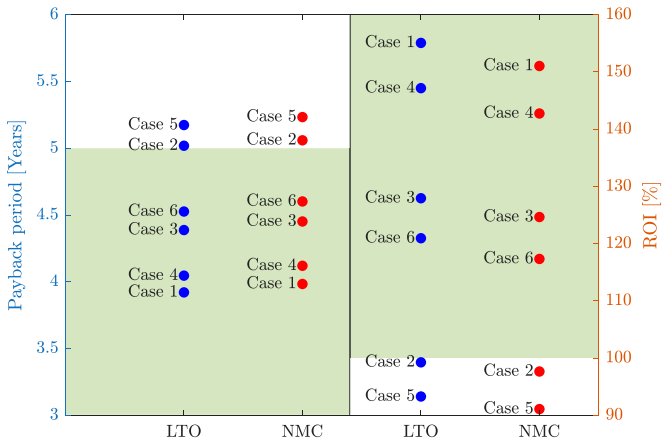

Fig. 9. Range of possible payback periods and ROI.

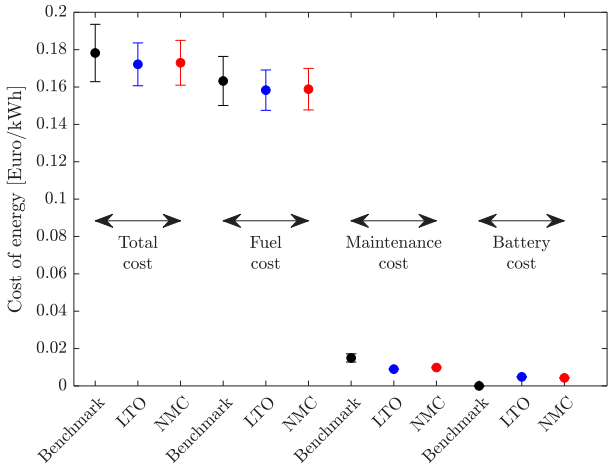

Fig. 10. Cost of energy per kWh.

The operational cost per kWh for the benchmark case is illustrated in the bars of Fig. 11. For scenarios $S_{i,j}$ with $i \in 2, 3$, the operational costs per kWh are higher compared to $i = 1$, indicating that load profiles 2 and 3 incur greater costs than load profile 1. The blue and red lines in the figure represent the operational expenses per kWh for hybrid power plants using LTO and NMC batteries, respectively. Notably, the highest cost savings per kWh are observed in load profiles 2 and 3, relative to profile 1. Furthermore, the cost per kWh remains relatively the same across different cases for LTO batteries within the same scenario. In contrast, for NMC batteries, the cost per kWh varies across both scenarios and cases, highlighting that the limited throughput of NMC batteries must be strategically managed depending on the scenario. The detailed contributions of operational expenses per kWh for different scenarios are depicted in Table A.7.

The split between fuel and maintenance savings relative to CAPEX, in Millions of euros, is illustrated in Fig. 12. For LTO batteries, the ratio of fuel savings to CAPEX ranges from 86.6–120.9%, while maintenance savings range from 111.5–140.7% of the CAPEX. In the case of NMC batteries, these ratios are 85.0–116.8% for fuel savings and 103.8–132.2% for maintenance savings. This distribution of savings relative to CAPEX indicates that both maintenance and fuel savings individually exceed the battery investment cost, thereby effectively paying for the batteries and more. Moreover, the maintenance savings in the case of LTO batteries is consistently more than those seen with NMC batteries. Indicating a difference in the operational strategy.

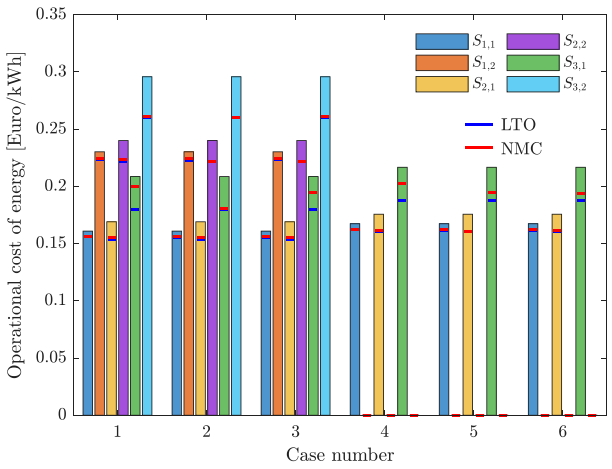

Fig. 11. Operational cost of energy per kWh. (For interpretation of the references to color in this figure legend, the reader is referred to the web version of this article.)

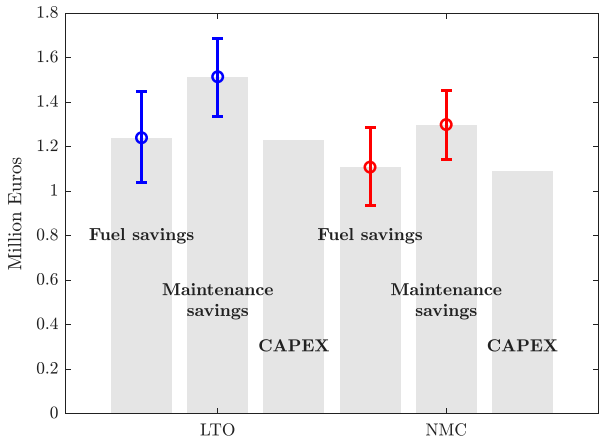

Fig. 12. Split of operational savings.

6.2. Implications on power plant operational strategy

The difference in operational expense savings discussed in Section 6.1 is further illustrated in Figs. 13(a) and 13(b), which depict the number of operational hours per day for DE-2 under LTO and NMC battery configurations, respectively. It is important to note that DE-1 remains ON at all times for all scenarios $S_{i,j}$ with $i, j \in [1, 2]$. Moreover, due to redundancy requirements, in the benchmark case, DE-2 is operational at all times.

A key observation is that under the LTO battery configuration, DE-2 is not operational in scenarios $S_{2,1}$ and $S_{2,2}$ across all cases. This indicates that DE-2 is not utilized under load profile 2. Additionally, a reduction in DE-2's operational hours is observed in scenario $S_{1,2}$ for cases 1–3, and in scenario $S_{1,1}$ for cases 5–6.

In contrast, with NMC batteries, DE-2 is OFF in scenario $S_{2,2}$ for cases 2 and 3. This is attributed to the higher cost per kWh associated with scenario $S_{2,2}$ relative to other scenarios. Specifically, in case 2 and case 3, the probabilities $P(S_{2,2})$ are approximately 4% and 9%, respectively, whereas in case 1, $P(S_{2,2})$ is around 13%. The lower probability in cases 2 and 3 means that scenario $S_{2,2}$ occurs less frequently, resulting in a reduced lifetime throughput requirement to turn OFF DE-2 in those cases. The operational strategy for DE-2 with a hybrid power

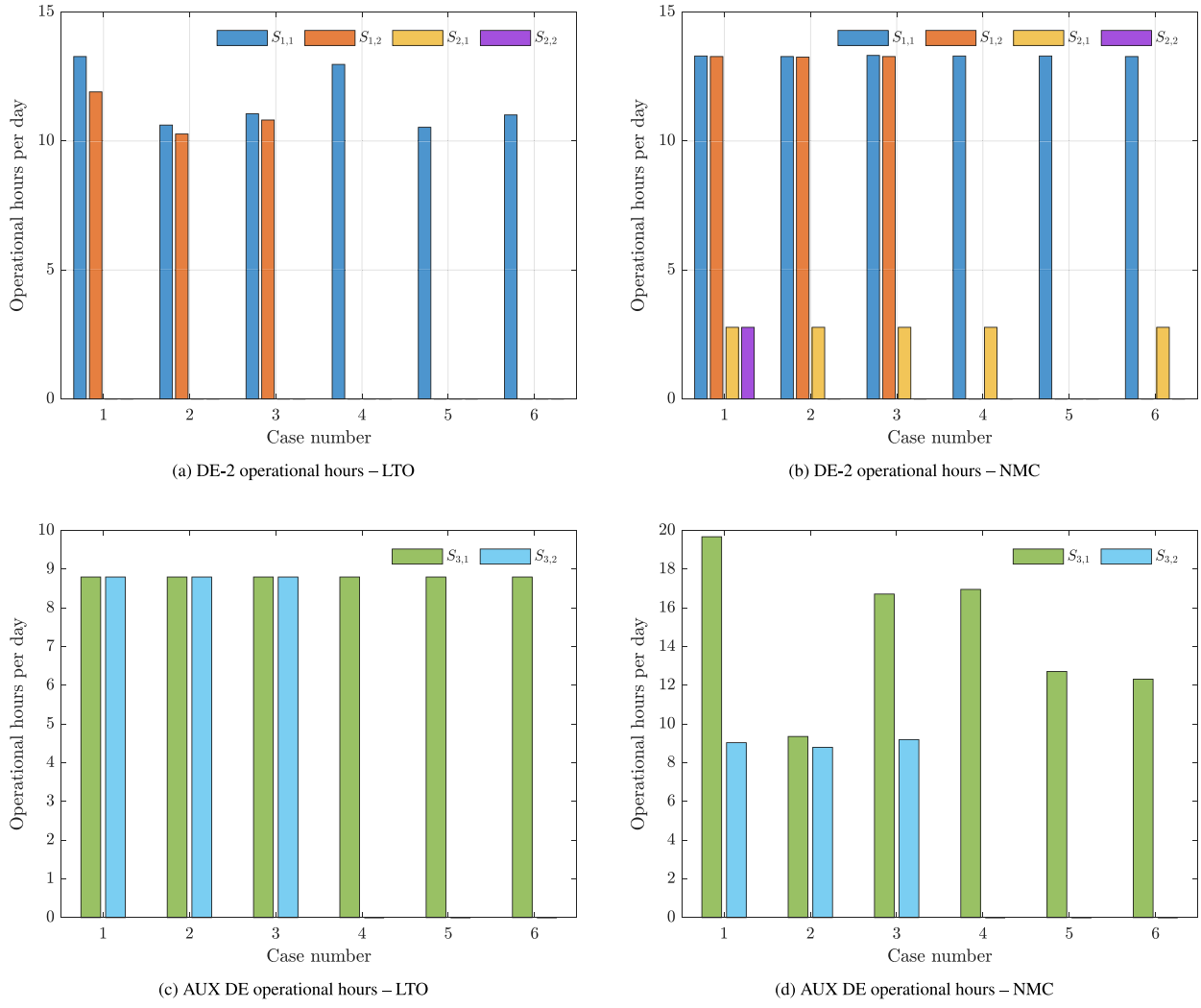

(a) DE-2 operational hours – LTO

(b) DE-2 operational hours – NMC

(c) AUX DE operational hours – LTO

(d) AUX DE operational hours – NMC

Fig. 13. Comparison of DE-2 and AUX DE operational hours across LTO and NMC cases.

plant of NMC batteries is consistent across cases for scenario $S_{1,j}$ across all cases. The data for Figs. 13(a) and 13(b) is tabulated in Table A.8.

The operation of the AUX DE for scenario $S_{3,j}$ in the case of LTO batteries is shown in Fig. 13(c). In the benchmark case, the AUX DE is always ON, i.e. the AUX DE is turned ON for 24 h for every operational day. The operation of the AUX DE in a hybrid power plant with LTO batteries is consistent across all the cases as shown in Fig. 13(c).

However, in the case of NMC batteries, the operation of the AUX DE for scenario-$S_{3,j}$ is not consistent as shown in Fig. 13(d). What can be observed is that the AUX DE is operational for longer periods in periods where the price of fuel is lower ($S_{3,1}$) as compared to when the price of fuel is higher ($S_{3,2}$) in case 1–3. The data for Figs. 13(c) and 13(d) is tabulated in Table A.9.

The power plant scheduling with LTO batteries for case 1, scenario $S_{1,1}$ is shown in Fig. 14(a). Where, SoE refers to the battery's State of Energy, defined as the amount of energy stored in the battery relative to its total capacity. The power plant is scheduled such that DE-2 is turned ON during periods of higher power demand (sailing). Here, the DE follows an ON/OFF strategy, where DE-2 is turned ON long enough for the battery to charge sufficiently. This ensures that when DE-2 is turned OFF, the battery and DE-1 can supply power to the system for at least 30 min before DE-2 is turned ON again. The battery's state of energy is also depicted, which shows the battery undergoes deep charge and discharge cycles.

The operation of the power plant is consistent for load profile 2 ($S_{2,j}$) for power plants with LTO batteries as discussed previously. The power split between DE-1 and the battery is shown in Fig. 14(b) for case 1 and scenario $S_{2,1}$. The role of the battery for this operational profile is to keep DE-2 OFF while shavings peak above the capacity of DE-1 and fill valleys to charge the battery.

The power demand when the vessel is not operational or at port in load profile 3 is significantly lower compared to load profiles 1 and 2. Consequently, the operational time of the AUX DE can be substantially reduced, as opposed to the current strategy, where it operates continuously during non-operational periods. An example of the power split between the AUX DE and the battery is shown in Fig. 14(c) for case 1, scenario $S_{3,1}$. The battery is charged in such a way that the AUX DE remains ON for at least 30 min and, once turned OFF, stays OFF for a minimum of 30 min.

Fig. 13(a) shows a difference in the operational hours of DE-2 between scenarios $S_{1,2}$ and $S_{1,1}$, attributed to the higher fuel price in $S1,2$. The corresponding power plant scheduling is shown in Fig. 14(d), and the difference can be compared with Fig. 14(a). During periods of low power demand, such as dumping or sailing, DE-2 is turned OFF for

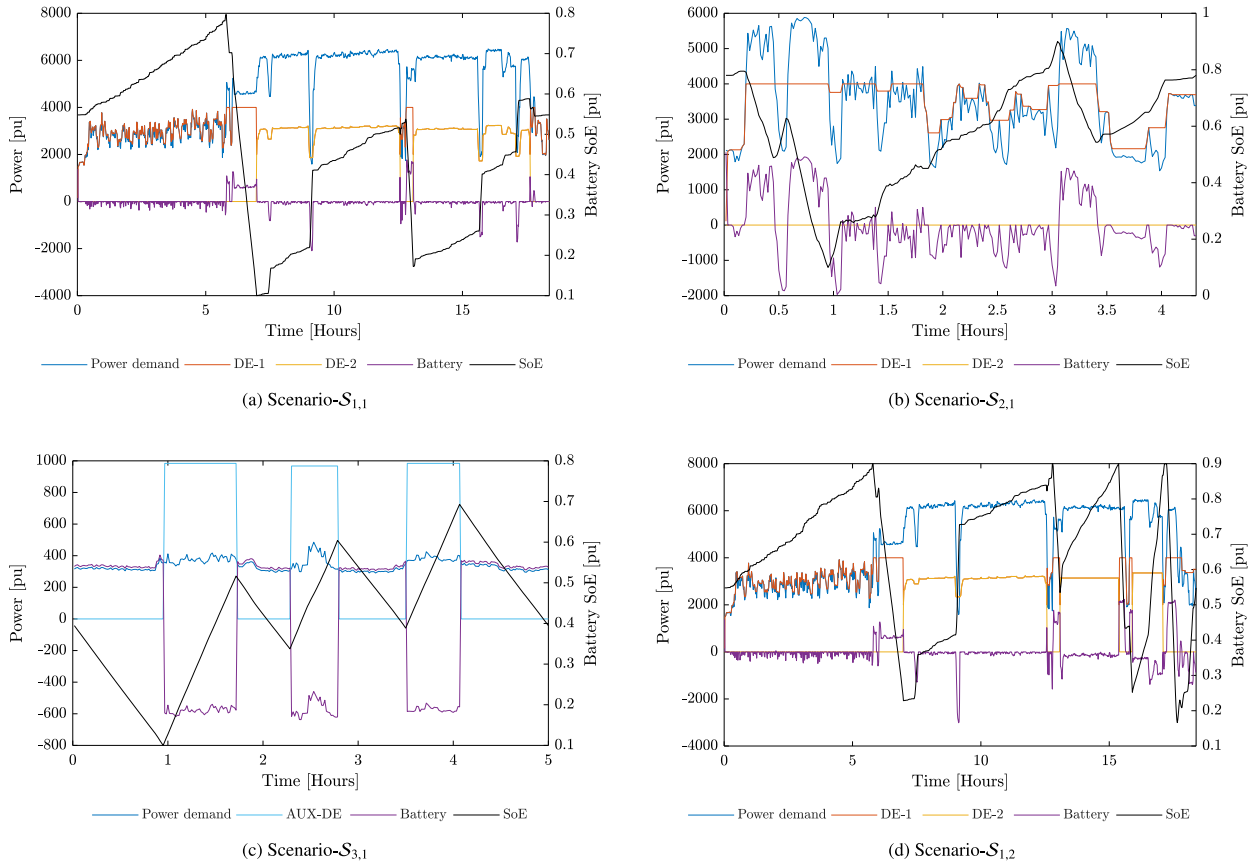

(a) Scenario-$\mathcal{S}_{1,1}$ (b) Scenario-$\mathcal{S}_{2,1}$

(c) Scenario-$\mathcal{S}_{3,1}$ (d) Scenario-$\mathcal{S}_{1,2}$

Fig. 14. Operational strategy for Case 1 - LTO batteries.

at least 30 min in $\mathcal{S}_{1,2}$. This strategy is not adopted in $\mathcal{S}_{1,1}$, where DE-2 remains operational at all times except during dredging. This contrast highlights the importance of utilizing battery throughput effectively, prioritizing periods where the operational cost per kWh of energy is high.

The operation of the power plant with NMC batteries is consistent across load profiles 1 and 2 in terms of the operational time of DE-2, as previously shown in Fig. 13(b). The power plant scheduling for Case 1, Scenario $\mathcal{S}_{1,1}$ is illustrated in Fig. 15(a). In this case, the scheduling strategy ensures that DE-1 remains operational during dredging, while DE-2 operates during dumping and low power demand periods, such as sailing, with a minimum ON duration of 30 min. This behavior resembles the operation observed with LTO batteries in Fig. 14(a). However, a key difference lies in the charging characteristics: LTO batteries support significantly higher charging rates, leading to deeper cycling and, consequently, a higher energy throughput compared to NMC batteries.

Similar to the first load profile, the operational strategy for the second load profile for NMC batteries also has a consistent power plant scheduling agnostic to fuel price and duration of each load profile ($P(S_{i,j})$). The operation of the power plant for scenario $\mathcal{S}_{2,1}$ is shown in Fig. 15(b). The power plant is scheduled with the battery in such a way that DE-2 is predominately turned OFF except for a short period of time during the dredging operation. Moreover, the state of energy does not increase as steeply in NMC batteries as compared to LTO batteries for the same scenario.

The operational hours of the AUX DE are significantly higher in cases 1, 3, 4, and 5 compared to cases 2 and 3. This is primarily because, in cases 1, 3, 4, and 5, the TSHD operates for a substantial portion of time in load profile 2. As a result, a large share of the allowable battery throughput is allocated to reducing the operational time of DE-2, leaving less throughput available for Scenario $\mathcal{S}_{3,1}$. This effect is seen in cases 1 and 3 under higher fuel prices, as seen in Scenario $\mathcal{S}_{3,2}$.

This contrast is illustrated in Figs. 15(c) and 15(d). In the low fuel price scenario ($\mathcal{S}_{3,1}$), the AUX DE is ON for significantly longer durations and is turned OFF only for the minimum required OFF time. Moreover, the loading on the AUX DE is lower than that observed in the higher fuel price scenario. In contrast, under the high fuel price scenario (Fig. 15(d)), the AUX DE operates closer to the minimum ON time and is turned OFF for durations much longer than the minimum OFF time.

The difference in operational strategy between LTO and NMC batteries arises primarily from the amount of available throughput. With increased operational time spent in load profile 2 (as seen in cases 1, 3, 4, and 6), the throughput available for load profiles 1 and 3 is reduced. Consequently, for NMC batteries, higher priority is given to scenarios with higher fuel prices in load profiles 1 and 3. Moreover, in the case of LTO batteries, the power plant scheduling remains consistent across load profiles 2 and 3. However, for load profile 1, higher throughput is allocated to periods with elevated fuel prices. The throughput used per hour of operation for different scenarios is presented in Fig. A.1.

Another important aspect of the battery requirements analysis is the power-to-energy ratio, as illustrated in Fig. 16. The charge and discharge power-to-energy ratios for LTO batteries are shown in Figs. 16(a) and 16(b). LTO batteries operate with a power-to-energy ratio below 0.5 for a significant portion of the time—≈ 55% during charging and ≈ 75% during discharging. This indicates that, although LTO

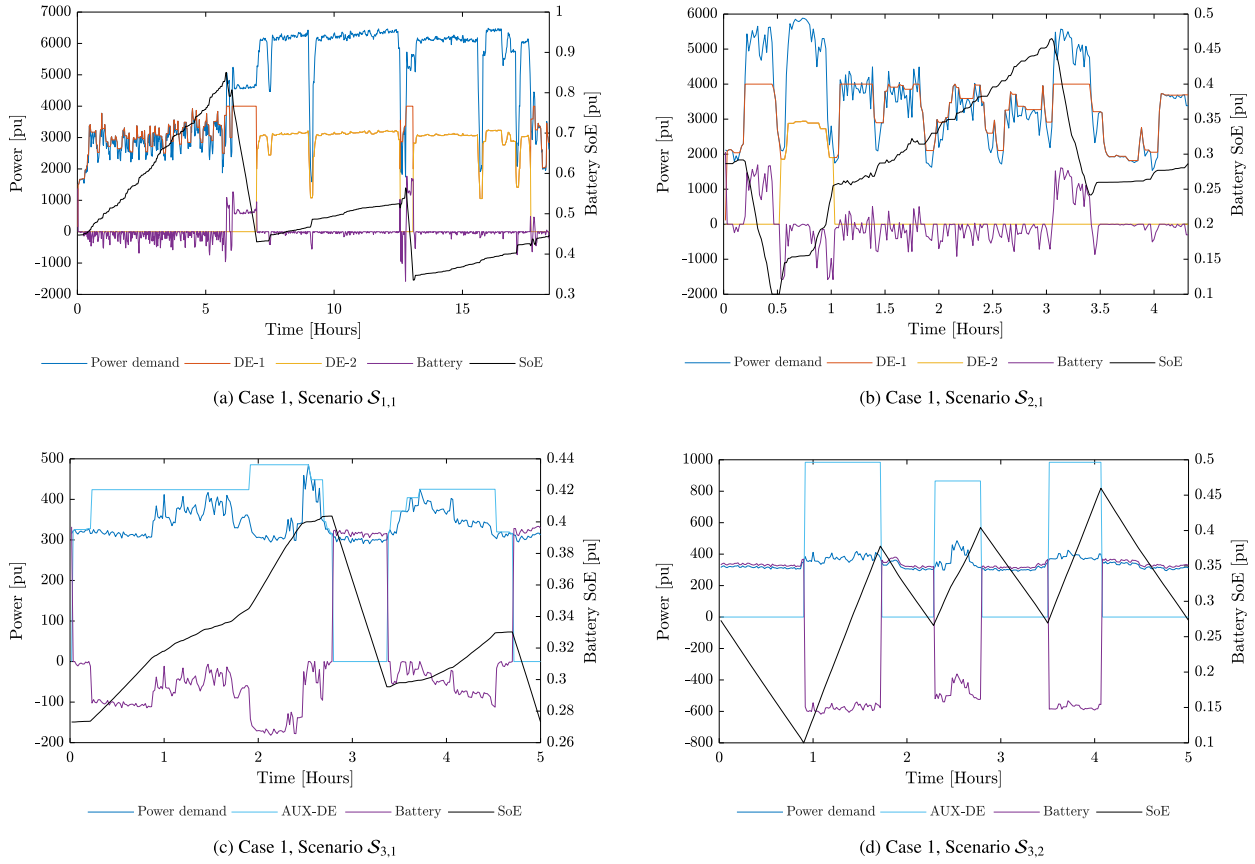

(a) Case 1, Scenario $\mathcal{S}_{1,1}$

(b) Case 1, Scenario $\mathcal{S}_{2,1}$

(c) Case 1, Scenario $\mathcal{S}_{3,1}$

(d) Case 1, Scenario $\mathcal{S}_{3,2}$

Fig. 15. Operational strategy for Case 1 - NMC batteries.

batteries are capable of fast charging and discharging, they are predominantly used at lower rates in practice. A similar trend is observed for NMC batteries (shown in Figs. 16(c) and 16(d)), with the ratio remaining below 0.5 for ≈ 95% of the time during charging and ≈ 86% during discharging. This further highlights that lower charge and discharge rates are commonly utilized, even for batteries designed for spinning reserve/ replacing a secondary DE. Moreover, this suggests that batteries designed for spinning or emergency reserve are often oversized relative to their actual usage. Since reserve functions are only required occasionally, typically during DE failures, the battery's ability to deliver high C-rates during these rare events could be sufficient, even if the supporting auxiliary systems are designed for lower C-rates. As a result, the extent of battery oversizing for reserve applications could be reduced.

7. Conclusion

The paper proposes a scenario-based stochastic framework for integrated battery sizing and power plant scheduling under uncertain maritime operations and fuel prices. Results show that hybridizing with LTO or NMC batteries offers economic and operational advantages over diesel-only systems. Battery capacities for both LTO and NMC are fixed across scenarios due to a reserve power constraint. The optimal sizes are 1066 kWh (LTO) and 1703 kWh (NMC), reflecting LTO's higher power density and throughput, which allow for deeper and more frequent cycling.

Hybrid systems consistently reduce lifetime costs (CAPEX + OPEX) compared to diesel-only setups. In all six cases, LTO configurations were cheaper than NMC. For example, in Case 1, the benchmark cost of €43.9M drops to €42.0M (LTO) and €42.3M (NMC). Similar trends appear across other cases. Payback periods confirm economic viability: LTO achieves payback in 3.92–5.01 years and NMC in 3.98–5.05 years. The ROI ranges from 93%–155% (LTO) and 91%–151% (NMC), driven by fuel and maintenance savings that offset battery costs. Hybrid systems also lower energy costs per kWh: €0.166–€0.178 (LTO), €0.167–€0.179 (NMC), vs. €0.171– €0.186 for diesel-only. Fuel remains the largest cost driver (>91%), but is significantly reduced in hybrid setups—especially with high fuel prices and short sailing profiles. Lower maintenance costs are also observed with LTO batteries, driven by reduced DE runtime.

Hybridizing with batteries enables more flexible and efficient operation. In short-sailing scenarios (load profile 2), DE-2 can remain OFF entirely with LTO across all cases—a major reduction from the 24-h operation in the benchmark. The NMC configuration, limited by lower throughput, cannot consistently achieve this.

Across scenarios, LTO reduces DE-2 usage to 0–13.3 h/day, depending on load and fuel price, with complete shutdowns in several high-fuel, low-load cases. NMC yields more moderate reductions, typically operating DE-2 for 2.8–13.3 h/day. Under low fuel prices, NMC systems keep DE-2 running longer to benefit from cheaper fuel, showing a more adaptive but constrained strategy.

During port operations (load profile 3), the AUX DE is always ON in the benchmark case. However, this can be turned OFF for extended periods. Hybridizing with LTO achieves more consistent shutdowns (≈8.8 h/day of AUX operation), while NMC ranges from 8.8 to 19.7 h/day, depending on the scenario.

One of the paper's key insights is that the operational strategy must be adapted to battery chemistry, the fuel price and load profile. LTO

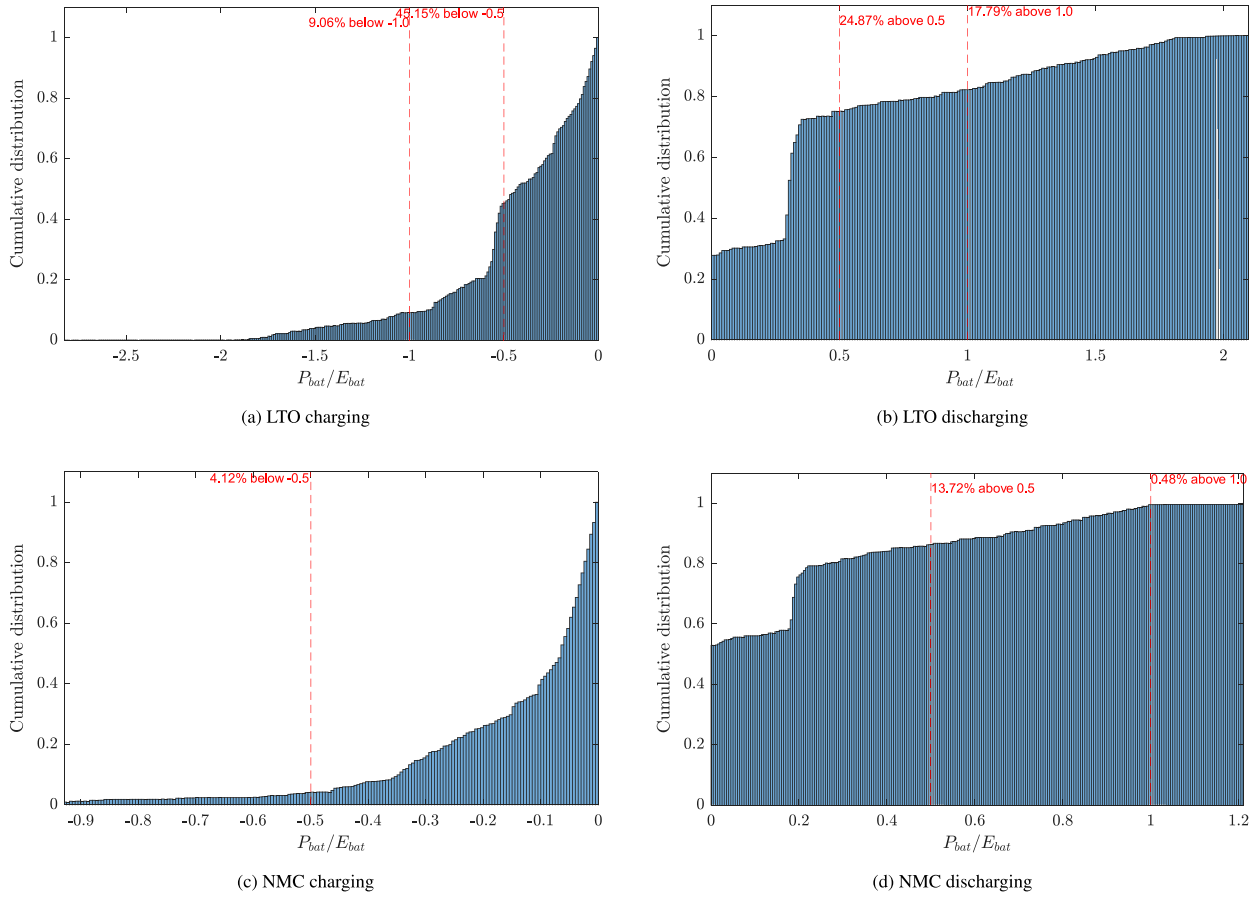

(a) LTO charging

(b) LTO discharging

(c) NMC charging

(d) NMC discharging

Fig. 16. Ratio of battery power to energy installed onboard.

batteries, with their superior throughput, allow consistent power plant scheduling across different scenarios. For NMC batteries, however, scheduling is more sensitive to fuel price and must prioritize high-cost periods to optimize battery use. This results in more variable DE usage in NMC-based systems.

The paper has certain limitations. Economically, it does not study and account for potential future reductions in battery and converter costs or the time-discounted value of capital expenditures. Technically, it assumes constant energy storage efficiency over a 10-year lifetime and does not consider the possibility of extended battery lifespans in future technologies. Furthermore, the fuel consumption curves of the DE have been linearized to ensure compatibility with the MILP formulation. This introduces approximations that does not capture the inherent non-nonlinearities of the fuel consumption curve.

In conclusion, the paper shows that hybridizing the power system of a TSHD leads to economic and operational improvements, with LTO batteries offering superior performance. These findings validate the use of a scenario-based optimization framework for designing and scheduling maritime hybrid systems under uncertainty. The consistent cost reductions through improved energy efficiency and reduced DE usage highlight the value of integrating batteries into maritime power plants.

CRediT authorship contribution statement

Sankarshan Durgaprasad: Writing – original draft, Visualization, Validation, Software, Methodology, Formal analysis, Conceptualization. **Andrea Coraddu:** Writing – review & editing, Visualization, Supervision, Methodology, Funding acquisition, Conceptualization. **Eben Heyneman:** Writing – review & editing, Resources, Data curation, Conceptualization. **Christof Lamproye:** Writing – review & editing, Resources, Data curation, Conceptualization. **Henk Polinder:** Writing – review & editing, Visualization, Supervision, Methodology, Funding acquisition, Conceptualization.

Declaration of competing interest

The authors declare that they have no known competing financial interests or personal relationships that could have appeared to influence the work reported in this paper.

Acknowledgments

This publication is part of the project Maritime Batteries with project number KICH1.KICH1.21.002 of the research programme KIC-Missie Emissieloze en Circulaire Scheepvaart 2021 which is financed by the Dutch Research Council (NWO).

Appendix. Tables and Figures

See Tables A.1–A.9 and Fig. A.1.

Table A.1
$P(S_{i,j})$ for different cases in percentage.

Scenario	Case					
	1	2	3	4	5	6
$S_{1,1}$	12.8	38.5	25.7	17.1	51.4	34.2
$S_{1,2}$	4.3	12.8	8.6	0	0	0
$S_{2,1}$	38.5	12.8	25.7	51.4	17.1	34.2
$S_{2,2}$	12.8	4.3	8.6	0	0	0
$S_{3,1}$	23.6	23.6	23.6	31.5	31.5	31.5
$S_{3,2}$	7.9	7.9	7.9	0	0	0

Table A.2
OPEX and lifetime costs for benchmark system in Million Euro.

Benchmark	Cost [Million Euro]					
Case	1	2	3	4	5	6
F^{cost}	40.1	45.9	43.0	37.5	42.9	40.2
M^{cost}	3.8	3.8	3.8	3.8	3.8	3.8
Lifetime	43.9	49.7	46.8	41.3	46.7	44.0

Table A.3
Lifetime costs in Million Euro.

Case	1	2	3	4	5	6
LTO	42.0	48.5	45.3	39.5	45.6	42.5
NMC	42.3	48.7	45.5	39.7	45.7	42.7

Table A.4
Life time cost split in Million Euro.

		Case					
		1	2	3	4	5	6
Benchmark	Fuel	40.1	45.9	43	37.5	42.9	40.2
	Maintenance	3.8	3.8	3.8	3.8	3.8	3.8
LTO	Fuel	38.7	44.8	41.7	36.1	41.8	39.0
	Maintenance	2.1	2.5	2.3	2.1	2.5	2.3
	Battery system	1.2	1.2	1.2	1.2	1.2	1.2
NMC	Fuel	38.9	44.9	41.9	36.3	42.0	39.1
	Maintenance	2.4	2.7	2.5	2.4	2.7	2.5
	Battery system	1.1	1.1	1.1	1.1	1.1	1.1

Table A.5
Payback time and ROI.

Case	1	2	3	4	5	6
Payback time [years]						
LTO	3.92	5.01	4.38	4.04	5.17	4.52
NMC	3.98	5.05	4.45	4.11	5.23	4.6
ROI [%]						
LTO	155	99	128	147	93	121
NMC	151	98	125	143	91	117

Table A.6
Cost per MWh in Euros.

Case	1	2	3	4	5	6
Total cost per MWh						
Benchmark	186	182	184	175	171	173
LTO	178	177	177	167	166	167
NMC	179	178	178	168	167	168
Fuel cost per MWh						
Benchmark	170	168	169	159	157	158
LTO	164	164	164	153	153	153
NMC	164	164	164	154	153	153
Maintenance cost per MWh						
Benchmark	16.1	13.9	14.9	16.1	13.9	14.9
LTO	9	9	9	9	9	9
NMC	10	9.7	9.8	10	9.7	9.8
Capex cost per MWh						
Benchmark	0	0	0	0	0	0
LTO	5.2	4.5	4.8	5.2	4.5	4.8
NMC	4.6	4	4.3	4.6	4	4.3

Table A.7
Operational cost per MWh per scenario Euros.

Case	1	2	3	4	5	6
Scenario	Benchmark					
S_1	160.9	160.9	160.9	167.4	167.4	167.4
S_2	230.2	230.2	230.2	0	0	0
S_3	169.1	169.1	169.1	175.7	175.7	175.7
S_4	240.1	240.1	240.1	0	0	0
S_5	209.9	209.9	209.9	218	218	218
S_6	297.5	297.5	297.5	0	0	0
Scenario	LTO					
S_1	155.9	154.9	155.1	162.2	161.2	161.4
S_2	223.6	222.9	223.2	0	0	0
S_3	154	154	154	160.3	160.3	160.3
S_4	222	222	222	0	0	0
S_5	180.1	180.1	180.1	187.5	187.5	187.5
S_6	260.5	260.5	260.5	0	0	0
Scenario	NMC					
S_1	155.9	155.9	155.9	162.3	162.2	162.3
S_2	224.2	224.2	224.2	0	0	0
S_3	155.5	155.5	155.5	161.9	161.9	161.9
S_4	223.7	222	222	0	0	0
S_5	200	181	194.5	202.8	194.8	194
S_6	261.1	260.5	261.3	0	0	0

Table A.8
Operational hours of DE-2 per day.

Case	1	2	3	4	5	6
Scenario	LTO					
S_1	13.3	10.6	11.1	13	10.5	11
S_2	11.9	10.3	10.8	0	0	0
S_3	0	0	0	0	0	0
S_4	0	0	0	0	0	0
Scenario	NMC					
S_1	13.3	13.3	13.3	13.3	13.1	13.3
S_2	13.3	13.3	13.3	0	0	0
S_3	2.8	2.8	2.8	2.8	2.8	2.8
S_4	2.8	0	0	0	0	0

Table A.9
Operational hours of AUX DE per day.

Case	1	2	3	4	5	6
Scenario	LTO					
S_1	8.8	8.8	8.8	8.8	8.8	8.8
S_2	8.8	8.8	8.8	0	0	0
Scenario	NMC					
S_1	19.7	9.4	16.7	17	12.7	12.3
S_2	9	8.8	9.2	0	0	0

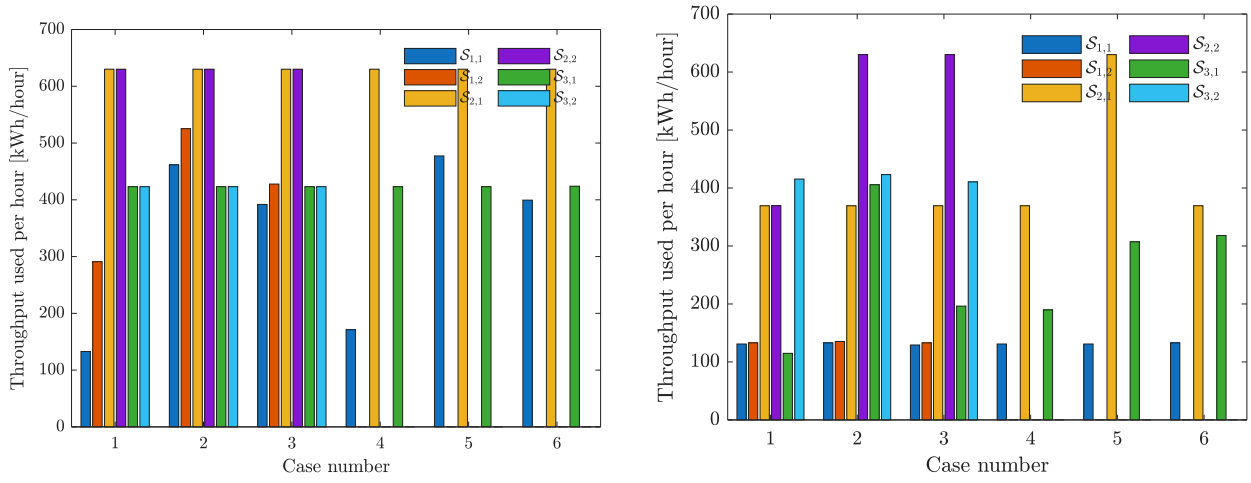

(a) LTO (b) NMC

Fig. A.1. Battery throughput per operational hour per case and scenario.

Data availability

Data will be made available on request.

References

[1] Helgesen H, Haugom GP, Sverud T, Henningsgård S, Gully B, Mjøs N, Langli AA, Frithiof N. Electrical energy storage for ships. Tech. Rep. Report No.: 2019-0217, Rev. 04, Document No.: 11B59ZDK-1, Høvik, Norway: DNV GL,European Maritime Safety Agency (EMSA); 2020, Prepared for the European Maritime Safety Agency, Cais do Sodré, 1249-206 Lisboa, Portugal. URL https://www.emsa.europa.eu.

[2] EST-Floattech. Electrification in aquaculture: Exposure in electric and hybrid solutions. 2023, URL https://www.est-floattech.com/wp-content/uploads/2023/07/Fishery-Aquaculture-exposure-in-Electric-and-Hybrid.pdf. [Accessed 06 March 2025].

[3] He W, Valøen LO, Olsen KV, Kjeka KM, Fredriksen BM, Petiteau M, Touat A, Såtendal H, Howie A, Howey D, et al. Lessons learned from the commercial exploitation of marine battery energy storage systems. J Energy Storage 2024;87:111440.

[4] Barone G, Buonomano A, Del Papa G, Maka R, Palombo A. Approaching zero emissions in ports: implementation of batteries and supercapacitors with smart energy management in hybrid ships. Energy Convers Manage 2024;314:118446.

[5] Hong SH, Kim DM, Kim SJ. Power control strategy optimization to improve energy efficiency of the hybrid electric propulsion ship. IEEE Access 2024;12:22534–45.

[6] Pang B, Liu S, Zhu H, Feng Y, Dong Z. Real-time optimal control of an LNG-fueled hybrid electric ship considering battery degradations. Energy 2024;296:131170.

[7] Zhang Y, Xue Q, Gao D, Shi W, Yu W. Two-level model predictive control energy management strategy for hybrid power ships with hybrid energy storage system. J Energy Storage 2022;52:104763.

[8] Xie P, Tan S, Guerrero JM, Vasquez JC. MPC-informed ECMS based real-time power management strategy for hybrid electric ship. Energy Rep 2021;7:126–33.

[9] Ship, Bunker. Rotterdam Bunker prices. 2025, URL https://shipandbunker.com/prices/emea/nwe/nl-rtm-rotterdam. [Accessed 06 March 2025].

[10] Durgaprasad S, Coraddu A, Polinder H. An analysis of maritime battery requirements and a decision tree for optimal chemistry selection. SSRN Electron J 2024. http://dx.doi.org/10.2139/ssrn.5118466, URL https://ssrn.com/abstract=5118466.

[11] Wang X, Shipurkar U, Haseltalab A, Polinder H, Claeys F, Negenborn RR. Sizing and control of a hybrid ship propulsion system using multi-objective double-layer optimization. IEEE Access 2021;9:72587–601.

[12] Fang S, Xu Y, Wang H, Shang C, Feng X. Robust operation of shipboard microgrids with multiple-battery energy storage system under navigation uncertainties. IEEE Trans Veh Technol 2020;69(10):10531–44. http://dx.doi.org/10.1109/TVT.2020.3011117.

[13] Hein K, Xu Y, Aditya V, Gupta AK. A probabilistic risk-averse approach for energy storage sizing in all-electric ship. J Energy Storage 2022;55:105392.

[14] Bordin C, Mo O. Including power management strategies and load profiles in the mathematical optimization of energy storage sizing for fuel consumption reduction in maritime vessels. J Energy Storage 2019;23:425–41.

[15] Kersey J, Popovich ND, Phadke AA. Rapid battery cost declines accelerate the prospects of all-electric interregional container shipping. Nat Energy 2022;7(7):664–74.

[16] Kistner L, Bensmann A, Hanke-Rauschenbach R. Potentials and limitations of battery-electric container ship propulsion systems. Energy Convers Manag: X 2024;21:100507.

[17] Rasul MJ, Kim J. Comprehensive review and comparison on battery technologies as electric-powered source in marine applications. J Energy Storage 2024;88:111509.

[18] Mutarraf MU, Terriche Y, Niazi KAK, Vasquez JC, Guerrero JM. Energy storage systems for shipboard microgrids—A review. Energ 2018;11(12):3492.

[19] Li X, Huang J, Zhang J, Zhou M, Wang T, Tang X, Lai J, Yang X. An adaptive multi-objective joint optimization framework for marine hybrid energy storage system design considering energy management strategy. J Energy Storage 2023;68:107689.

[20] Akbarzadeh M, De Smet J, Stuyts J. Battery hybrid energy storage systems for full-electric marine applications. Process 2022;10(11):2418.

[21] Tummakuri V, Chelliah TR, Ramesh US. Sizing of energy storage system for a battery operated short endurance marine vessel. In: 2020 IEEE international conference on power electronics, smart grid and renewable energy. PESGRE2020, 2020, p. 1–6. http://dx.doi.org/10.1109/PESGRE45664.2020.9070268.

[22] Mashayekh S, Wang Z, Qi L, Lindtjorn J, Myklebust T-A. Optimum sizing of energy storage for an electric ferry ship. In: 2012 IEEE power and energy society general meeting. 2012, p. 1–8. http://dx.doi.org/10.1109/PESGM.2012.6345228.

[23] van Veldhuizen B, van Biert L, Ünlübayir C, Visser K, Hopman J, Aravind PV. Component sizing and dynamic simulation of a low-emission power plant for cruise ships with solid oxide fuel cells. Energy Convers Manage 2025;326:119477.

[24] Wu S, Li T, Xu F, Chen R, Zhou X, Wang B. Configuration size optimization of gas-electric hybrid power systems on ships considering energy density and engine load response. Energy Convers Manage 2024;301:118069.

[25] Kistner L, Bensmann A, Hanke-Rauschenbach R. Optimal design of power gradient limited solid oxide fuel cell systems with hybrid storage support for ship applications. Energy Convers Manage 2021;243:114396.

[26] Haseltalab A, van Biert L, Sapra H, Mestemaker B, Negenborn RR. Component sizing and energy management for SOFC-based ship power systems. Energy Convers Manage 2021;245:114625.

[27] Dotto A, Satta F. Techno-economic optimization of hybrid-electric power plants onboard cruise ships. Energy Convers Manag: X 2023;20:100436.

[28] Mylonopoulos F, Durgaprasad S, Coraddu A, Polinder H. Lifetime design, operation, and cost analysis for the energy system of a retrofitted cargo vessel with fuel cells and batteries. Int J Hydrog Energy 2024;91:1262–73.

[29] Dolatabadi A, Mohammadi-Ivatloo B. Stochastic risk-constrained optimal sizing for hybrid power system of merchant marine vessels. IEEE Trans Ind Inform 2018;14(12):5509–17. http://dx.doi.org/10.1109/TII.2018.2824811.

[30] Alharbi H, Bhattacharya K. Stochastic optimal planning of battery energy storage systems for isolated microgrids. IEEE Trans Sustain Energy 2017;9(1):211–27.

[31] Nguyen TA, Crow ML. Stochastic optimization of renewable-based microgrid operation incorporating battery operating cost. IEEE Trans Power Syst 2015;31(3):2289–96.

[32] Jordehi AR, Tabar VS, Mansouri S, Nasir M, Hakimi S, Pirouzi S. A risk-averse two-stage stochastic model for planning retailers including self-generation and storage system. J Energy Storage 2022;51:104380.

[33] Balderrama S, Lombardi F, Riva F, Canedo W, Colombo E, Quoilin S. A two-stage linear programming optimization framework for isolated hybrid microgrids in a rural context: The case study of the "El Espino" community. Energy 2019;188:116073.
[34] Soares J, Canizes B, Ghazvini MAF, Vale Z, Venayagamoorthy GK. Two-stage stochastic model using benders' decomposition for large-scale energy resource management in smart grids. IEEE Trans Ind Appl 2017;53(6):5905–14.
[35] Zhang H, Grossmann IE, Tomasgard A. Decomposition methods for multi-horizon stochastic programming. Comput Manag Sci 2024;21(1):32.
[36] Gurobi Optimization, LLC. Release notes for Gurobi 12.0. 2025, URL https://docs.gurobi.com/projects/optimizer/en/current/reference/releasenotes.html. [Accessed 1 August 2025].
[37] Kanchiralla FM, Brynolf S, Malmgren E, Hansson J, Grahn M. Life-cycle assessment and costing of fuels and propulsion systems in future fossil-free shipping. Environ Sci Technol 2022;56(17):12517–31.